

Review

# Group 4 Metal-Based Metal—Organic Frameworks for Chemical Sensors

Souvik Pal, Sheng-Sheng Yu  and Chung-Wei Kung 

Department of Chemical Engineering, National Cheng Kung University, 1 University Road, Tainan City 70101, Taiwan; 11008083@email.ncku.edu.tw

\* Correspondence: sssyu@mail.ncku.edu.tw (S.-S.Y.); cwkung@mail.ncku.edu.tw (C.-W.K.)

**Abstract:** Metal-organic frameworks (MOFs) have attracted great attention for their applications in chemical sensors mainly due to their high porosity resulting in high density of spatially accessible active sites, which can interact with the aimed analyte. Among various MOFs, frameworks constructed from group 4 metal-based (e.g., zirconium, titanium, hafnium, and cerium) MOFs, have become especially of interest for the sensors requiring the operations in aqueous media owing to their remarkable chemical stability in water. Research efforts have been made to utilize these group 4 metal-based MOFs in chemosensors such as luminescent sensors, colorimetric sensors, electrochemical sensors, and resistive sensors for a range of analytes since 2013. Though several studies in this subfield have been published especially over the past 3–5 years, some challenges and concerns are still there and sometimes they might be overlooked. In this review, we aim to highlight the recent progress in the use of group 4 metal-based MOFs in chemical sensors, and focus on the challenges, potential concerns, and opportunities in future studies regarding the developments of such chemically robust MOFs for sensing applications.

**Keywords:** cerium-based MOF; electrochemical sensor; gas sensor; hafnium-based MOF; optical sensor; resistive sensor; titanium-based MOF; zirconium-based MOF



**Citation:** Pal, S.; Yu, S.-S.; Kung, C.-W. Group 4 Metal-Based Metal—Organic Frameworks for Chemical Sensors. *Chemosensors* **2021**, *9*, 306. <https://doi.org/10.3390/chemosensors9110306>

Academic Editor: Boris Lakard

Received: 4 October 2021

Accepted: 26 October 2021

Published: 28 October 2021

**Publisher's Note:** MDPI stays neutral with regard to jurisdictional claims in published maps and institutional affiliations.



**Copyright:** © 2021 by the authors. Licensee MDPI, Basel, Switzerland. This article is an open access article distributed under the terms and conditions of the Creative Commons Attribution (CC BY) license (<https://creativecommons.org/licenses/by/4.0/>).

## 1. Introduction

The sensitive, selective, and accurate detection of various environmental pollutants in the gas, vapor, and liquid phase is a very important task for environment monitoring, food safety, medical diagnosis, occupational safety, toxic/hazardous chemical management, and industrial process management [1–3]. Most of the commercially available sensors utilize inorganic-based semiconductors or organic polymers as active materials, which can react or absorb the targeted analyte. During this process, rapid changes in photophysical, electrical, or mechanical properties of these materials are of interest for a good performing sensor. The degree of the changes usually depends on the concentration of analytes and various physical and chemical characteristics of both the analytes and the active materials, such as electron accepting-donating ability, acidity or basicity, permeability, hydrogen bonding ability, electrostatic interaction, and  $\pi$ - $\pi$  stacking (See Figure 1) [1]. Detection of ultra-trace level analytes with a high sensitivity and a high accuracy towards a range of environmental and biological samples is usually essential for an efficient sensor and its commercialization. In addition, the design of portable, easy-to-handle, fast, inexpensive, and highly sensitive devices is also needed for the development of commercially available chemical sensors [1,3].

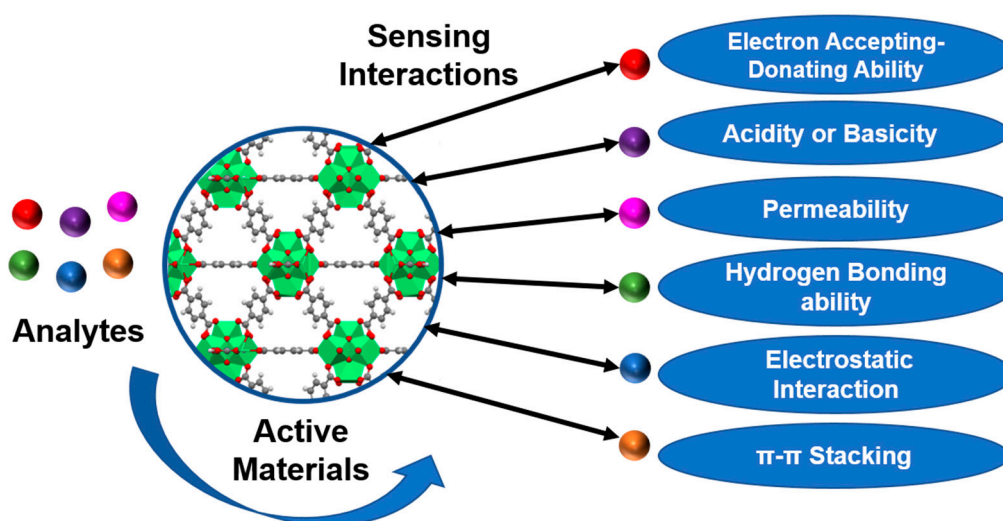


**Figure 1.** A schematic illustration of the interactions involved in the detection of various analytes.

In this regard, as a relatively new class of potential active materials for chemical sensors, metal-organic frameworks (MOFs), also known as porous coordination polymers (PCPs), have been intriguing, and frequently applied by several research groups. MOFs are an emerging class of nanoporous materials that are constructed from metal-based nodes and organic linkers [4–6]. Compared to other categories of nanoporous materials such as carbons, mesoporous silica, and zeolites, MOFs possess several unique characteristics including regular pore size, interconnected porosity, ultrahigh specific surface area, and tunable chemical functionality within the entire porous framework. Such appealing features have rendered the developments of various MOF structures and MOF-based materials for a range of applications such as gas storage [7,8], separation [9,10], catalysis [11–14], drug delivery [15,16], energy storage [17–19], energy conversion [20,21], and optoelectronic devices [22,23] over the past two decades. As a variety of chemically active units for sensing purposes can be incorporated within the entire framework structure by either selecting the proper building blocks for synthesizing MOFs or performing post-synthetic modifications (PSM) [24,25], and the interconnected porosity of MOFs is expected to provide a facile mass transport of the targeted molecules within the entire framework, the use of MOFs for chemical sensors has attracted great attention [1]. However, most MOFs show relatively poor chemical stabilities in water compared to other nanoporous materials [26,27], which strongly limits the use of pristine and structurally robust MOFs in sensing applications for environmental or biological samples in early years.

To tackle the challenge for utilizing pristine MOFs in environmental or biological sensing purposes, the development and use of chemically robust MOFs, especially those highly stable in water, are thus required. Utilizing high-valent metal ions and carboxylate-based linkers to construct MOFs is one of the popular methods to increase the stability of MOFs [26,27]. High-valent metal ions contain high charge density, which helps to form strong metal-to-ligand bonds when the same linkers and coordinating topology are presented. Moreover, high-valent metal ions need more linkers to coordinate for the overall charge balance, which repels the attack of the guest molecules like water; this characteristic results in the formation of highly stable MOFs [27–29]. Such causes thus motivated the design and synthesis of highly stable group 4 metal-based MOFs. Group 4 metal-based MOFs belong to the frameworks constructed from the nodes composed of high-valent metal ions, e.g., Ti(IV), Zr(IV), Hf(IV), or Ce(IV), and usually carboxylate-based linkers. Owing to their exceptional chemical stabilities in water under a wider range of pH [27,28,30], such MOFs are considered as attractive candidates for chemical sensing purposes. The first Zr(IV)-based MOF (Zr-MOF), UiO-66 (UiO = University of Oslo), was discovered by Lillerud et al. in 2008 and has also been known for its exceptional thermal and chemical stabilities [31]. In UiO-66, the secondary building unit (SBU) consisting of

$Zr_6O_4(OH)_4$  is bonded with twelve 1,4-BDC (BDC = benzene-dicarboxylate) ligands to form a framework with the face-centred cubic (fcu) topology. Since then, a large number of Zr-MOFs possessing various coordinating topologies, pore sizes, and unique chemical functionalities have been designed and synthesized [32]. Zirconium and hafnium belong to the same group in the periodic table with the similar electronic configurations ( $d^0$ ) and closely identical ionic radius owing to f-block contraction. Therefore, Hf(IV)-based MOFs (Hf-MOFs) usually show similar physical properties and structures compared to their Zr-based isostructural MOFs synthesized in a same reaction condition. Such isostructural Hf-MOFs can be usually synthesized under a similar synthetic environment by replacing  $Zr^{4+}$  metal ions with  $Hf^{4+}$  ions [33]. Hf-MOF is more stable compared to Zr-MOF due to the highest Hf-O bond strength compared to Zr-O. The dissociation enthalpy of Hf-MOF is  $802 \text{ kJ mol}^{-1}$ , which is higher than Zr-MOFs ( $776 \text{ kJ mol}^{-1}$ ) [30]. The first Ti(IV)-carboxylate-based MOFs (Ti-MOFs), MIL-125(Ti), was reported in 2009 by Férey and coworkers [34]. However, since  $Ti^{4+}$  shows completely distinct electronic configuration and ionic radius compared to  $Zr^{4+}$  and  $Hf^{4+}$ , the number of reported Ti-MOFs with permanent porosity is still quite limited compared to those of Zr-MOFs and Hf-MOFs. Though cerium does not belong to the group 4 metals in the periodic table, Ce(IV)-based MOFs (Ce-MOFs) emerging in recent years are known to possess the comparable chemical stabilities of Zr-MOFs in water and the redox activity of their metal-based nodes [35,36]. Owing to the same electronic configuration ( $d^0$ ) of  $Ce^{4+}$  compared to those of  $Zr^{4+}$  and  $Hf^{4+}$ , the isostructural Ce-MOFs, such as Ce-based UiO-66, have been widely reported in literature [35,37,38]. The historical progress in the design, synthesis, and resulting crystalline structures of these group 4 metal-based MOFs can be found in detail in some recent review articles [28,32,36]. As these group 4 metal-based MOFs are water-stable, the use of such MOFs for multiple types of chemical sensors operated in aqueous environments, such as optical sensors, electrochemical sensors, and resistive sensors, has been widely reported since 2013 (see Figure 2). Although significant efforts have been made in this subfield in recent years, some challenges and concerns are still there and sometimes they might be overlooked. In this review, we aim to highlight the recent progress in the use of group 4 metal-based MOFs in chemical sensors especially with the focus emphasized on the challenges, potential concerns, and opportunities in future studies for the developments of such chemically robust MOFs for sensing applications.

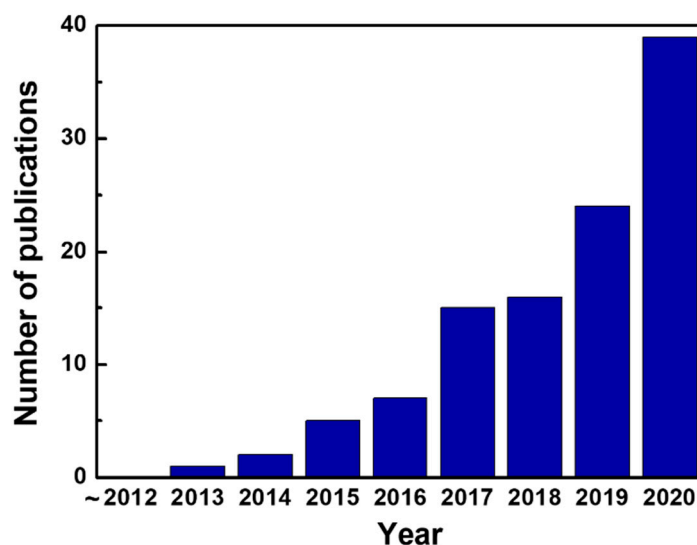


**Figure 2.** The number of publications reporting the use of Zr-MOFs, Ti-MOFs, Hf-MOFs, or Ce-MOFs for sensors published in each year, obtained from Web of Science database.

## 2. Synthesis and Characterizations of Group 4 Metal-Based MOFs

Most group 4 metal-based MOFs are usually synthesized by solvothermal methods. In such processes, the organic ligand or linker and metal salt are dissolved in a solvent within a Teflon-lined autoclave or a glass vial, and the resulting mixture reacts at a definite temperature to yield the solid MOF crystals. The porous MOF solid can be obtained after successive washing with the solvent used during MOF growth followed by the proper solvent exchange before drying to activate the MOF [39]. However, owing to the strong metal-oxygen bonds presented in these group 4 metal-based MOFs, the directly synthesized MOFs usually exhibit poor crystallinity due to the rapid nucleation process. In this regard, modulated synthesis is commonly used for the preparation of group 4 metal-based MOFs [28]. A modulator with the identical chemical functionality as the organic linker is introduced during MOF growth to slow the interaction between the metal ions and organic linkers in order to get the well crystalline frameworks. Commonly used modulators for synthesizing carboxylate-based group 4 metal-based MOFs include formic acid, acetic acid, benzoic acid, and trifluoroacetic acid. As the synthetic strategies and structures of these MOFs are not the main focuses of this article, the details regarding the design and synthesis of various group 4 metal-based MOFs can be found in previously published review articles [28,30,32,36].

For the common characterizations of MOFs, X-ray diffraction (XRD) is generally used to probe the crystallinity of a MOF. By comparing the experimental powder or thin-film XRD pattern with the simulated pattern obtained from the single-crystal diffraction data, the crystalline phase of the MOF sample can be determined. However, it should be noted that the purity of a MOF cannot be verified solely by XRD, as the amorphous phase in the sample is not detectable by XRD. Gas adsorption-desorption experiments are usually conducted to gauge the porosity of a MOF, and the surface morphology as well as the uniformity of the MOF sample can be characterized by electronic microscopes. Details regarding the use of various techniques to characterize MOF materials is beyond the scope of this article and can be found in previously published work [40,41].

## 3. Chemical Stabilities of Group 4 Metal-Based MOFs toward the Use in Chemosensors

Before the use of a MOF for a targeted sensing application, it is crucial to ensure the structural integrity of the MOF in the environments for that sensing purpose. Otherwise, the structural degradation of the framework during the sensing operations may result in the unstable or less reproducible performances of the obtained chemosensor. Moreover, some MOFs can also encounter structural degradation and become MOF-derived materials during exposure to the environments used for applications, which results in the use of MOF-derived metal oxides or hydroxides as the active materials rather than the real structurally well-defined MOFs [42–44]. Such instability of MOFs during applications becomes more difficult to distinguish in the electrochemical sensing systems since the structural degradation of MOFs and the formation of MOF-derived materials may solely occur on the surface [45]. As mentioned in the previous section, group 4-metal-based MOFs are generally stable in water, which makes them desirable as chemosensors in aqueous media. The strong coordination between the M(IV)-based clusters and carboxylate groups of the linkers renders these MOFs highly stable in acidic solutions [28]. Thus, several commonly reported Zr-MOFs and Ti-MOFs such as UiO-66 and its derivatives [46], MOF-808 [47], PCN-222 (also known as MOF-545) [48,49], NU-1000 [27,50], and MIL-125(Ti) [34] show similar chemical stabilities in aqueous solutions with the pH ranging from 1 to around 9–11. It was even reported that a Zr-MOF, PCN-222/MOF-545, can show structural integrity after treating with concentrated hydrochloric acid [48]. For Ce-MOFs, the similar but slightly less chemical stabilities compared to their Zr-based isostructural frameworks in acidic aqueous solutions were also reported [35,51]. Frameworks like Zr-MOFs can even maintain their crystalline structures after exposure to H<sub>2</sub>S gas [52,53], indicating the feasibility of utilizing such MOFs for reductive gas sensors. However, the replacement of

the carboxylate-based linkers by  $\text{OH}^-$  ions can occur within these group 4 metal-based MOFs in strong alkaline solutions, which results in the degradation of these MOFs in base solutions [27,28]; such degradations usually cause the evolution of MOF-derived metal oxides or hydroxide species. As some chemosensors need to be operated in alkaline solutions, the chemical stabilities of these group 4 metal-based MOFs under the pH of the sensing environment should be first considered before use.

In addition to the pH values of the sensing environments, another crucial factor to be considered is the stabilities of these group 4 metal-based MOFs in the presence of ionic species. Even though such MOFs are generally stable in water, the presence of strongly coordinated ions in the environments for sensing applications may still result in the degradation of MOFs [27]. For example, phosphate ions belong to one common type of ionic species presented in biological systems, which makes the use of phosphate buffer solutions (PBS) become quite common in the studies of various chemosensors for biological and biosensing applications. However, even under a neutral or low pH, the degradation of such group 4 metal-based MOFs can occur in PBS owing to the strongly coordinating nature of the phosphate ions [27]. Thus, the MOF-derived metal phosphate can be formed in such buffer solutions [54]. Even one of the most stable group 4 metal-based MOFs, UiO-66, was reported to lose around 90% of its porosity after being treated with PBS under a neutral pH [55]. Thus, the chemical stabilities of the selected group 4 metal-based MOF in the buffer solutions required for the targeted sensing operations must be carefully considered if the formation of MOF-derived materials is not desired. A recent study has shown that the Zr-MOFs demonstrate remarkable stabilities in the buffer solutions containing 4-(2-hydroxyethyl)piperazine-1-ethane sulfonic acid (HEPES) or diluted 2-amino-2-(hydroxymethyl)-1,3-propanediol (TRIS) as well as in the unbuffered sodium chloride solutions [55]. Some early studies as well as our recent work also suggested that the buffer compound possessing a similar chemical structure of HEPES, 3-morpholinopropane-1-sulfonic acid (MOPS), can be used with various Zr-MOFs while keeping the structural integrities of the frameworks [56,57]. Thus, for utilizing group 4 metal-based MOFs in chemical sensors, these buffer solutions are more appropriate compared to the commonly used PBS. Since the chemical stabilities of various structurally distinct group 4 metal-based MOFs within different buffered systems were barely investigated in literature so far, employing characterization methods such as X-ray diffraction, nitrogen adsorption and X-ray photoelectron spectroscopy after the targeted sensing application are recommended in order to ensure the stability of the issued MOFs during the sensing operations.

In the following section, we will introduce the basic principles regarding the rational design of group 4 metal-based MOFs for various kinds of chemosensors, including optical sensors, electrochemical sensors, and resistive sensors. The progress in the developments of these group 4 metal-based MOFs for the use in such chemosensors and the corresponding examples will also be highlighted.

## 4. Applications of Group 4 Metal-Based MOFs for Chemosensors

### 4.1. Optical Sensors

Optical chemical sensors rely on the optical changes of the systems upon the exposure to the targeted analytes [58]. As most analytes do not show optical responses by themselves, the use of an active material that can selectively reveal optical changes upon the exposure to the analyte is usually required for the design of optical chemosensors [58]. Depending on the sensing mechanisms, various types of optical responses probed by spectroscopic measurements can be utilized, including infrared (IR) and ultraviolet-visible (UV-vis) absorbance and fluorescence signal. Such optical sensors can be utilized to detect metal ions or organic pollutants in aqueous solutions, monitor the concentrations of biomolecules in biological systems, and detect toxic gases such as  $\text{H}_2\text{S}$  and  $\text{NO}_2$  in gaseous environments. As MOFs in general possess high specific surface area and interconnected porosity, the presence of spatially dispersed active sites immobilized within the entire MOF framework is expected to maximize the amount of accessible active sites within

per volume of the material that can be exposed to the analyte molecules coming from the external environment. This attractive characteristic has thus motivated the design and use of MOFs and MOF-based materials for a range of optical chemical sensors since early years [59]. The use of water-stable group 4 metal-based MOFs further facilitated the applications of such MOFs in various optical chemosensors for aqueous samples. Among various types of optical chemosensors utilizing group 4 metal-based MOFs, a majority of examples consist of luminescent sensors. The emission properties of MOFs may be attributed to the (I) ligand-based luminescent, including ligand-to-metal charge transfer (LMCT), metal-to-ligand charge transfer (MLCT), and ligand-localized emission, (II) metal ion-based emission, (III) absorbate-based emission, and (IV) functionalized fluorescent probes within the MOF [60,61]. It should be noted that for Zr-MOFs, Ti-MOFs, and Hf-MOFs, their metal-based clusters show neither significant absorbance within the visible region nor the fluorescent property. Thus, the presence of the optically active moieties within such MOFs by either incorporating them as a part of the organic linkers for MOF synthesis or installing them in the MOF by post-synthetic modifications (PSM) is usually required for use in optical sensors. The following sections will highlight the use of group 4 metal-based MOFs in a variety type of optical sensors. As most of these reported examples utilized Zr-MOFs, the optical sensors using Zr-MOFs will be classified into multiple subsections according to the analytical purposes.

#### 4.1.1. Zr-MOFs for Optical Ion Sensors

Owing to their exceptional chemical stability in water as well as their relatively large pore sizes compared to those of the common ionic species presented in aqueous solutions, Zr-MOFs have attracted great attention for the applications of ion sensors. Due to the  $d^0$  electronic configuration of zirconium metal ions, luminescent Zr-MOFs were usually prepared by combining such metal ion-based clusters with the  $\pi$ -conjugated luminescent organic linkers. For example, an luminescent Zr-MOF,  $Zr_6O_4(OH)_7(H_2O)_3(BTBA)_3$  (BUT-39), was synthesized by using a T-shaped  $\pi$ -conjugated ligand 4,4',4''-(1H-benzo[d]imidazole-2,4,7-triyl)tribenzoic acid ( $H_3BTBA$ ) with  $ZrCl_4$  for the selective detection of  $Cr_2O_7^{2-}$  in water [62]. BUT-39 was found to exhibit a strong fluorescence emission originated from the linker-centric luminescent properties, and the luminescence significantly decreased in the presence of  $Cr_2O_7^{2-}$  ions. In general, there are four possible pathways for the fluorescence quenching in MOFs, including the interaction between organic ligand and analyte, ion exchange between the analyte and central metal ion, competitive absorption of the excitation light between the active material and the targeted object, and the collapse of the framework during sensing [63]. In this case, the competitive absorption and energy transfer between  $Cr_2O_7^{2-}$  and BUT-39 are the main causes for the quenching effect on the luminescence of BUT-39 [62]. Similarly, a pyridyl-functionalized Zr-MOF (UiO-66@N) showed an excellent fluorescent sensing ability towards  $Fe^{3+}$  ions with a detection limit of 0.69 ppm following the similar mechanism [64]. Another common type of luminescent organic linkers used in Zr-MOFs belongs to the porphyrins, which have been known for their remarkable fluorescent properties. The free nitrogen in the porphyrin could bind to the guest metal ions, which could result in a decrease in fluorescence upon the exposure to the targeted ions. For example, a porphyrinic Zr-MOF, NU-902, was reported to exhibit significant fluorescence quenching in the presence of cadmium metal ion ( $Cd^{2+}$ ) with a detection limit of 0.3 ppb; the MOF was further immobilized within a polymeric membrane to develop the sensing devices [65]. Biswas et al. reported a Zr-MOF (DUT-52) constructed from the 1-(2,2,2-trifluoroacetamido) naphthalene-3,7-dicarboxylic acid ( $H_2NDC-NHCOCF_3$ ) linker, which showed a highly sensitive and selective turn-on fluorescence toward cyanide ( $CN^-$ ) anion [66]. The  $H_2NDC-NHCOCF_3$  ligand contains a  $\pi$ -conjugated naphthalene ring and trifluoroacetamido group as the binding sites for  $CN^-$ . Despite the  $\pi$ -conjugated ring, DUT-52 showed a weak fluorescence due to the presence of the electron-withdrawing trifluoroacetamido group. The strong affinity between  $CN^-$  and the trifluoroacetamide groups is feasible for the formation of a cyanohydrin adduct through nucleophilic addition.

Therefore, photo induced electron transfer (PET) between the electron-withdrawing group and the aromatic system was inhibited. As a result, a remarkable enhancement of the fluorescence intensity was observed. Similarly, Zhou and coworkers developed a turn-on MOF-based sensor for  $\text{CN}^-$  detection by utilizing a MOF (PCN-700) containing anthracene as the fluorophore and hemicyanine as the recognition moiety (Figure 3a) [67]. The hemicyanine moiety could bond with  $\text{CN}^-$  selectively, affecting the energy transfer between the fluorophore and recognition moiety; the turn-on fluorescence was thus observed.

In addition to designing the Zr-MOFs constructed from luminescent linkers, PSM is another straightforward approach for introducing emissive moieties in MOFs. Several organic functional groups like amines, hydroxyl, halides, azides, and imines can be incorporated into the MOF pores through PSM [68]. In this regard, the uncoordinated amine group ( $-\text{NH}_2$ ) was usually used for further PSM since it can be easily fitted into different MOFs directly during the MOF synthesis. For example, a commonly seen Zr-MOF, UiO-66- $\text{NH}_2$  [46], was frequently used for the preparation of fluorescence sensors. The  $\pi$ -conjugated aromatic ring itself provides a strong fluorescence emission. Meanwhile, the free amine group can be involved in various chemical reactions to prepare the recognition sites of the guest molecules via PSM. For instance, UiO-66- $\text{NH}_2$ -SA (SA = salicylaldehyde) was synthesized by incorporating SA within UiO-66- $\text{NH}_2$  through a Schiff-base condensation reaction [63]. Bidentate ligand sites (N and O) could be generated in the framework, which could coordinate to  $\text{Al}^{3+}$  and show enhanced fluorescence intensity upon the exposure to  $\text{Al}^{3+}$  ions. Likewise, Yan et al. introduced imidazole moiety into UiO-66- $\text{NH}_2$  (named UiO-66- $\text{NH}_2$ -IM) via PSM based on a Schiff-base reaction to develop the bifunctional fluorescent probe for the detection of  $\text{S}_2\text{O}_8^{2-}$  and  $\text{Fe}^{3+}$  [69]. In addition, Yan and coworkers demonstrated the post-synthetic functionalization of citric acid into UiO-66- $\text{NH}_2$  via a condensation reaction. The resulting MOF (UiO-66- $\text{NH}_2$ -Cit) was employed as a potential luminescent sensor for the detection of  $\text{NO}_2^-$  in food preservatives [70]. Another functionalized structurally homologous Zr-MOF, named UiO-66- $\text{N}_3$  ( $\text{Zr}_6\text{O}_4\text{OH}_4(\text{C}_8\text{H}_3\text{O}_4\text{-N}_3)_6$ ), was further post-synthetically incorporated with phenylene acetylene by a Cu-catalyzed click reaction to obtain a triazole moiety-based MOF. The resulting MOF could be utilized in the luminescent detection of  $\text{Hg}^{2+}$  owing to the luminescent quenching caused by the coordination of  $\text{Hg}^{2+}$  ions on the triazole moiety [71]. It should be noted that beyond UiO-66-type Zr-MOFs, other candidates with distinct topologies and larger pore sizes should also allow the PSM to incorporate structurally well-defined emissive moieties within Zr-MOFs, but reports on the use of such MOFs for ion sensors are still quite limited.

Another common strategy for designing Zr-MOFs to be applied in ion sensors is to encapsulate or embed the fluorophores into the MOF during the MOF growth. With this approach, various fluorophores, such as Rhodamine B (RhB), 7-amino-4-methylcoumarin, resorufin, fluorescein (FL), and eosin Y (EY), can be incorporated into Zr-MOFs [72–74]. For example, Wang et al. demonstrated the encapsulation of RhB into a Zr-MOF, UiO-(OH) $_2$ , by growing the MOF in the presence of RhB (Figure 3b) [75]. The resulting material (UiO-(OH) $_2$ @RhB) was found to show two fluorescence peaks at 500 and 583 nm originated from the MOF linker and RhB, respectively. Due to the binding between the free hydroxyl group of the linker and  $\text{Al}^{3+}$  ions, such a dual-emitting composite could be applied for the turn-on ratiometric fluorescent sensor to detect  $\text{Al}^{3+}$  with a low detection limit of 10 nM [75]. Similarly, another Zr-MOF incorporated with RhB was also reported to detect  $\text{Fe}^{3+}$  ion, nitenpyram (pesticide), and 4-nitrophenol (nitroaromatic explosives) [76]. Zhang et al. also selected a series of Zr-MOFs constructed from naphthalene-based linkers for the encapsulation of RhB to prepare the dual-emissive composites, and such Zr-MOF-based composites were utilized in the detection of  $\text{Fe}^{3+}$  and  $\text{Cr}_2\text{O}_7^{2-}$  [72]. In addition to RhB, other dyes were also employed for the similar purpose. For example, 7-amino-4-methylcoumarin and resorufin were incorporated into a Zr-MOF, MOF-801, for the selective detection of  $\text{Cr}_2\text{O}_7^{2-}$  [72]. The fluorescein (FL) incorporated Zr-MOF, FL@UiO-67, was employed for the detection of  $\text{Al}^{3+}$  ions with a detection limit of 3.3 nM [73]. A dual-emitting composite, EY@Zr-MOF, was also prepared to detect  $\text{Fe}^{3+}$ ,  $\text{Cr}_2\text{O}_7^{2-}$ , and 2-nitrophenol [74]. It can be

found that this technique is effective not only for ion sensors but also for the detection of various organic pollutants, including nitroaromatics and pesticides. Compared to PSM, the encapsulation of fluorophores during MOF growth allows the incorporation of fluorophores possessing larger molecular sizes than the pore size of the MOF. However, the interaction and affinity between the Zr-MOF and the incorporated fluorophore should always be considered with care to prevent the leaching of the luminescent probes during the solution-phase sensing applications.

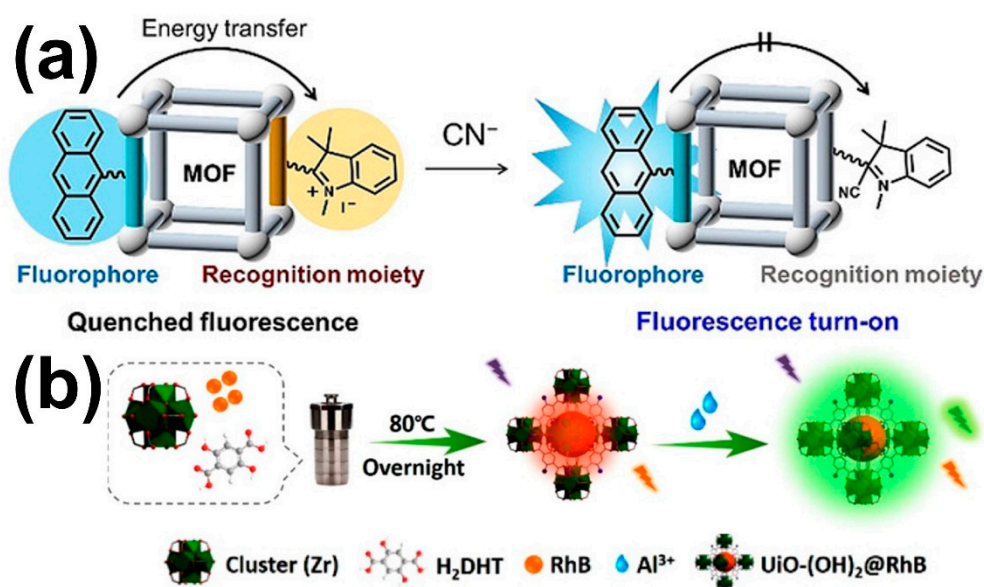


**Figure 3.** (a) Schematic representations for the design of a turn-on fluorescence sensor in multicomponent MOFs by integrating a fluorophore and a recognition moiety. Reprinted with permission from [67]. Copyright (2020) John Wiley and Sons. (b) Synthesis of UiO-(OH)<sub>2</sub>@RhB for the detection of Al<sup>3+</sup> ions. Reprinted with permission from [75]. Copyright (2020) American Chemical Society.

#### 4.1.2. Zr-MOFs for Optical Sensors toward Organic Pollutants

With increasing concerns for human health, food safety, homeland security, industrial monitoring, and environmental safety, there is a great interest in the fast, accurate, selective, and sensitive detection of various organic pollutants, including nitro explosives (NAEs), poly aromatic hydrocarbon (PAHs), volatile organic compounds (VOCs), organophosphates pesticides (OPPs), endocrine disrupting chemicals (EDCs), and antibiotics. Among various NAEs, 2,4,6-trinitrophenol (TNP), 2,4-dinitrophenol (DNP), 4-nitrophenol (4-NP) are widely used in military goods and industrial chemicals. As the detection of such organic pollutants in aqueous samples is required, the water-stable Zr-MOFs with luminescent characteristics thus became the attractive candidates. It should be noted that the selection of the Zr-MOF with the pore size larger than the targeted analyte is crucial since some organic pollutants, drugs, and antibiotics possess large molecular sizes. The fluorescent active sites within the highly porous MOF are accessible to the analyte molecules only when the facile mass transfer of the analyte through the MOF pore is allowed.

In 2016, Biswas et al. demonstrated the use of a Zr-MOF constructed from the 4,4'-(benzo[c][1,2,5]thiadiazole-4,7-diyl)dibenzoic acid (H<sub>2</sub>BTDB) linker for the selective luminescent detection of TNP [77]. As shown in Figure 4, the absorption band of TNP overlaps with the emission band of the linker-based fluorophore, which results in the energy transfer from the linker to the analyte and the decreased fluorescence upon the exposure of the MOF to TNP. Additionally, it was reported that the electrostatic interaction between the hydroxyl group of TNP and the nitrogen atoms of the linker might increase the quenching ability. Wang and coworkers also reported a similar electrostatic interaction, where a tetraphenylethene functionalized Zr-MOF could detect both the TNP and DNP in an alcoholic medium [78]. Another early example was demonstrated by

Li and coworkers, which showed that two fluorescent Zr-MOFs constructed from 5'-(4-carboxyphenyl)-2',4',6'-trimethyl-[1,1':3',1''-terphenyl]-4,4''-dicarboxylic acid ( $H_3CTTA$ ) and 6,6',6''-(2,4,6-trimethylbenzene-1,3,5-triyl)tris(2-naphthoic acid) ( $H_3TTNA$ ) linkers could be used to selectively detect TNP and 4-NP due to the energy transfer between the linkers and analytes [79]. Similarly, a recent example also showed that by incorporating the luminescent amine-functionalized carbon quantum dots into UiO-66, the resulting composite could be applied for the selective detection of 4-NP [80]. On the other hand, in a very recent study, Poddar and coworkers demonstrated the use of a UiO-67 derivative constructed from the 2-phenylpyridine-5,4'-dicarboxylate linker in the selective detection of TNP by Raman intensity quenching approaches. Such a new method based on Raman spectroscopy provides the non-invasive and non-destructive techniques in the subfield of MOF-based optical sensors [81].

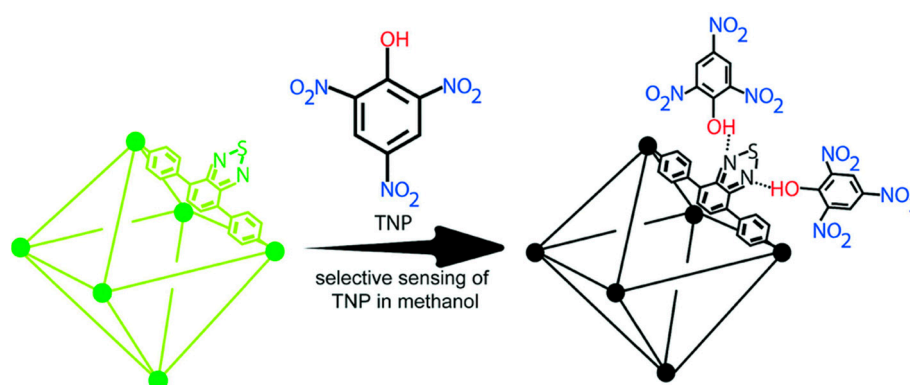


**Figure 4.** Schematic representation for the selective detection of TNP by a Zr-MOF constructed from  $H_2BTDB$  linker. Reprinted with permission from [77]. Copyright (2016) Royal Society of Chemistry.

For the solution-phase optical detection of PAHs, VOCs, pesticides, EDCs, and other small organic hazardous chemicals via using Zr-MOFs, the reported examples are still rare so far. As pyrene belongs to a notable type of fluorophore, a mesoporous Zr-MOF constructed from the pyrene-based linker, NU-1000, was recently reported as the potential fluorescent sensor to detect various PAHs [82]. VOCs are mainly harmful and odorous substances, such as aromatics, hydrocarbons, olefins, and amines. In 2016, Kaskel et al. reported the vapochromic luminescence of a Zr-MOF constructed from the 9-fluorenone-2,7-dicarboxylic acid linker, DUT-122(Zr), and such luminescent characteristics could be used for sensing non-polar aromatic and non-aromatic solvent vapors [83]. A few studies have also reported the use of Zr-MOFs for the solution-phase detection of VOCs. For example, in 2017, Wang, Li, and coworkers reported the use of a fluorescent UiO-68-type Zr-MOF containing mixed linkers, UiO-68-osdm, for the luminescent detection of dissolved amines; the detection of amines in gas phase by this MOF was also successfully demonstrated [84]. Another notable example is the Eu(III)-incorporated UiO-66-NH<sub>2</sub>, which was reported to exhibit dual-emitting fluorescent properties and could optically detect formaldehyde in aqueous solutions [85]. Another common hazardous chemical, phenol, was also reported to be detected by an luminescent tetrazine linker-based Zr-MOF owing to the drastically quenched fluorescence upon the exposure of the MOF to the electron-rich phenol [86]. For the detection of pesticides, a very recent study reported by Xing, Chen, and coworkers showed that an eosin Y (EY)-encapsulated Zr-MOF, EY@DUT-52, could be used to detect a range of pesticides in ethanol-based solutions owing to the quenching of energy transfer from the Zr-MOF to EY in the presence of the pesticides [87]. On the other hand, Ruan et al. reported the first example of enzyme-assisted MOF-based fluorescent sensor for EDCs. With the assistance of horseradish peroxidase and H<sub>2</sub>O<sub>2</sub>, diethylstilbestrol (DES, a common synthetic estrogen) could be oxidized to a quinone and accordingly detected by the stilbene-based fluorescent Zr-MOF [88].

Luminescent Zr-MOFs have been directly used as the active materials for the detection of various drugs or antibiotics including aspirin, tetracycline, clenbuterol, and chloramphenicol [89,90]. For instance, in an early study, UiO-66-NH<sub>2</sub> was reported for the fluorescent detection of aspirin [91]. A common antibiotic tetracycline (TC) can also be recognized as well as removed from the solutions by Zr-MOFs for environmental safety [92]. For example, a sharp luminescence quenching of a Zr-MOF, PCN-128Y, was observed in the presence of tetracycline [93]. The high adsorption of TC in the MOF and the PET process from the MOF linker to TC are both the causes of such a quenching phenomenon. It should be noted that as buffer solutions are usually needed for such sensing purposes, the chemical stability of Zr-MOFs in the selected buffer must be considered, as discussed previously in Section 3.

#### 4.1.3. Zr-MOFs for Optical Sensors toward Biomolecules

Biomolecules including glutathione (GSH), cysteine (Cys), homocysteine, and neurotransmitters such as dopamine play important roles in biological processes occurring in various living organisms. The amounts of such biomolecules beyond limits disrupt the biological process, which is harmful to the body. Thus, it is essential to detect such compounds with a high accuracy. Zr-MOFs and related materials have been directly utilized in the optical detection of biomolecules owing to their well-known chemical stability. However, the use of Zr-MOFs as well as other group 4 metal-based MOFs for such purposes has more challenges and limitations compared to that for the aforementioned sensing purposes, since a range of large biomolecules possess larger molecular sizes than the pore sizes of Zr-MOFs. In addition, the presence of phosphate ions, which is common in several biologically environments, can cause the structural degradation of most Zr-MOFs (see Section 3 for details). With the targeted biomolecules larger than the pore size, only the active sites near the surface of the MOF crystals can be involved in the sensing reaction, rendering the role of the MOF porosity in such sensing processes unclear. Furthermore, the stability of the selective Zr-MOF in the targeted biological samples for sensing must be considered first before use.

In 2014, Jiang et al. first demonstrated the use of a Zr-MOF, UiO-66-NH<sub>2</sub>, as an effective fluorescent sensing platform to detect DNA [94]. Tris buffer solutions were used to ensure the structural integrity of the MOF, and it was reported that the hydrogen bonding interaction between the amine functional group in MOF and DNA is responsible for such a sensing phenomenon. As UiO-66-NH<sub>2</sub> generally shows fluorescence emission around 500 nm and its amine group interacts with some specific analytes strongly, the material has been widely utilized to optically detect a range of biomolecules such as NO [95], dopamine [96], and GSH [96]. On the other hand, another early example demonstrated by Dong, Zhang, and coworkers synthesized the UiO-type Zr-MOFs constructed from the linkers grafted with the maleimide moiety (Mi-UiO-66 and Mi-UiO-67). The exposure of such MOFs to GSH or Cys would cause the chemical transformation of the moiety to its thiol adduct with enhanced fluorescence responses, which renders the use of such MOFs for turn-on detection of GSH and Cys [97]. Based on the same concept, another UiO-type MOF (UiO-68-An/Ma) was recently synthesized (Figure 5) [98]. The MOF contains binary linkers with one fluorophore (anthracene) based linker and another acceptor-functionalized linker (maleimide). The system showed weak fluorescence originated from the pseudo-intramolecular PET between anthracene and maleimide. Upon the exposure of the analyte, the maleimide group could further react with thiol compound (2-mercaptoethanol) through the thiol-ene reaction in water medium that can turn on the fluorescence signal.

As mentioned earlier, rather than utilizing the Zr-MOF with fluorescent linkers, another common approach is to incorporate the fluorescent probe or other active species into Zr-MOF by PSM. For example, the carboxymethyl  $\beta$ -cyclodextrin ( $\beta$ -CMCD) was post-synthetically functionalized within a luminescent mesoporous Zr-MOF, NU-1000. Rhodamine 6G (Rh6G) was further incorporated into the resulting NU-1000-CMCD, which caused the inhibition of fluorescence signal due to the energy transfer between NU-1000-

CMCD and Rh6G. Such a material was utilized in the optical detection of cholesterol, an essential lipid presented in blood samples, due to the binding of cholesterol with  $\beta$ -CMCD to turn on the fluorescence [99]. On the other hand, Li, Xia, and coworkers demonstrated the incorporation of luminescent Eu(III) sites into a Zr-MOF by PSM, and the obtained material (UiO-66(COOH)<sub>2</sub>, Zr-MOF: Eu<sup>3+</sup>) was used for the visual identification of bilirubin (BR) in human serum [100]. Another recent example is regarding the use of PSM performed in a Zr-MOF to detect 2,6-pyridinedicarboxylic acid (DPA), which is a suitable biomarker for the determination of Bacillus species that are related to an acute disease named anthrax. In this work, a Tb(III)-functionalized Zr-MOF, Tb<sup>3+</sup>@UIO-67, was directly used as the luminescent sensor for DPA, and a low detection limit of 36 nM was achieved [101].

Colorimetric sensors based on Zr-MOFs were also developed for detecting biomolecules. In a recent study demonstrated by Li, Sun, and coworkers, a composite material composed of UiO-66-NH<sub>2</sub>, gold nanoparticles, and decorated single-stranded-DNA was synthesized and applied for human semen identification [102]; significant color change was observed upon the exposure of the composite material to the proteins presented in semen.

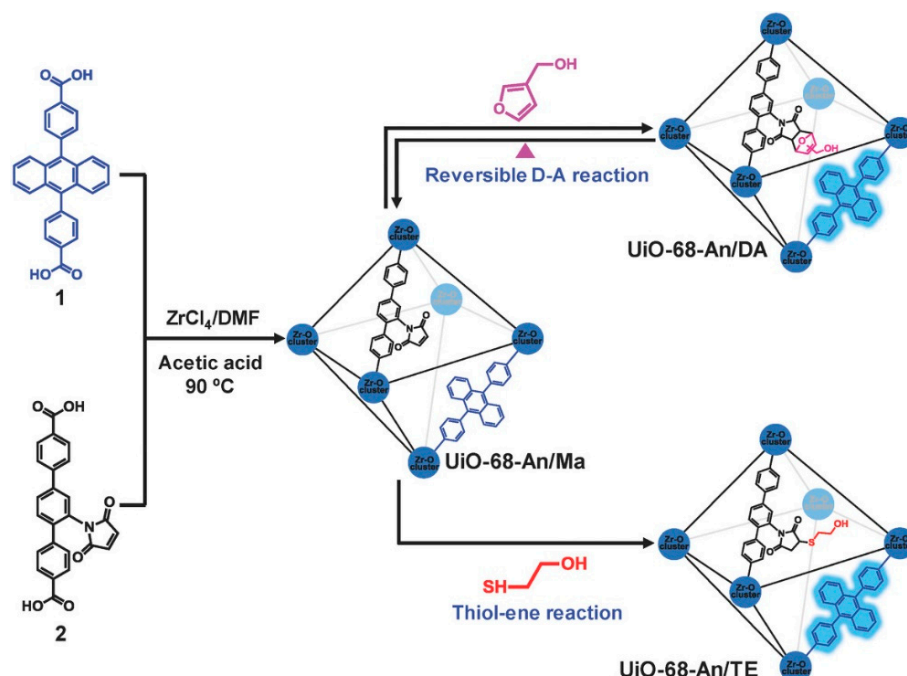


**Figure 5.** Synthesis of UiO-68-An/Ma and tuning the fluorescent PET in the MOF through the reversible D–A reaction or thiol-ene reaction. The topology is shown in the simplified form as an octahedral cage. Reprinted with permission from [98]. Copyright (2018) John Wiley and Sons.

#### 4.1.4. Zr-MOFs for Optical Sensors toward Inorganic Molecules

In an early work published in 2014, the UiO-66 derivative constructed from the dihydro-1,2,4,5-tetrazine-3,6-dicarboxylate linker has been used for the reversible colorimetric sensors toward nitrous gases, as demonstrated by Kaskel et al.; sharp and reversible color changes between pink and yellow were observed during such processes due to the redox activity of the linker [103]. In addition to the detection in gas phase, Zr-MOFs have also been applied for the optical detection of inorganic small molecules such as hydrazine, H<sub>2</sub>O<sub>2</sub>, and H<sub>2</sub>S in aqueous samples. For example, in 2018, Biswas et al. first demonstrated the use of a Zr-MOF, UiO-66-(NO<sub>2</sub>)<sub>2</sub>, to detect H<sub>2</sub>S in HEPES buffer solutions [104]. The -NO<sub>2</sub> group presented in the MOF linker could be converted to amine by reacting with H<sub>2</sub>S, enhancing the fluorescence intensity of the MOF upon the exposure to H<sub>2</sub>S. A very recent study demonstrated by the same group also reported the similar sensing mechanism occurring in an azide-functionalized Zr-MOF (DUT-52-N<sub>3</sub>) [105]. It should be noted that since such Zr-MOFs are chemically stable in HEPES buffer solutions and H<sub>2</sub>S, it was reported

that these MOFs can well preserve their crystalline structures after H<sub>2</sub>S sensing. In addition, colorimetric detection of H<sub>2</sub>S was also successfully performed by using UiO-66-(NO<sub>2</sub>)<sub>2</sub> under daylight. On the other hand, Cao et al. reported the use of a dual-linker Zr-MOF containing pyrene-based and porphyrin-based linkers to selectively detect H<sub>2</sub>S and its derivatives (S<sup>2-</sup>) in the aqueous solutions. The Zr-MOF could show turn-on fluorescence upon the exposure to H<sub>2</sub>S gas or S<sub>2</sub><sup>-</sup>-containing aqueous solutions [106].

Hydrazine and its derivatives are well-known reagents that can cause severe environmental and health issues. In 2018, Guo and coworkers demonstrated the incorporation of the fluorescent Eu(III) sites into a Zr-MOF, UiO-66-(COOH)<sub>2</sub>, by PSM, and the resulting material could detect hydrazine hydrate in ethanol solutions [107]; the strong luminescent response originated from Eu(III) sites could be significantly quenched by the analyte. Another example also showed the use of a phthalimide-functionalized UiO-66 for the turn-on detection of hydrazine. The phthalimide group could be converted into the amine group upon the exposure to hydrazine, resulting in the enhanced fluorescent signal [108]. Moreover, such a fluorescent probe successfully detected hydrazine in MDAMB-231 breast cancer cells without cellular cytotoxicity.

Another type of notable inorganic species that can be optically detected by Zr-MOFs belong to reactive oxygen species (ROS), including hydrogen peroxide (H<sub>2</sub>O<sub>2</sub>) and superoxide radical anion (O<sub>2</sub><sup>-</sup>). In 2018, Biswas et al. first demonstrated the use of a boronic acid functionalized Zr-MOF, Zr-UiO-66-B(OH)<sub>2</sub>, for the fluorometric detection of H<sub>2</sub>O<sub>2</sub> in HEPES buffer medium at pH 7.4 with a remarkable detection limit of 0.015 μM (Figure 6) [109]. In this case, the B(OH)<sub>2</sub> groups can react with H<sub>2</sub>O<sub>2</sub>, resulting in the formation of -OH groups showing significant emission at 426 nm. The same research group also reported two Zr-MOFs (Zr-UiO-66-NH-CH<sub>2</sub>-Py and UiO-66-NH-SO<sub>2</sub>-Ph-NO<sub>2</sub>) for the fluorometric sensing of reactive superoxide radical anion (O<sub>2</sub><sup>-</sup>) in aqueous and methanolic medium, respectively [110,111]. Furthermore, UiO-66-NH-SO<sub>2</sub>-Ph-NO<sub>2</sub> also shows fluorescent turn-on properties toward acetylacetone in the organic solutions. Another notable example was reported by Dong, Li, and coworkers, which demonstrated the use of a Zr-MOF constructed from the phenothiazine-decorated benzimidazole bridging dicarboxyl linker (UiO-68-PT) for the optical detection of another ROS, hypochloric acid (HClO) [112]. The phenothiazine moiety of UiO-68-PT showed a sharp white-to-red reversible color change in the presence of HClO (oxidant) and Vitamin C (reductant) in water. Moreover, the authors also demonstrated the fabrication of mixed-matrix membranes (MMM) by using poly(vinyl alcohol) and UiO-68-PT for the easy colorimetric detection of HClO in aqueous solutions.

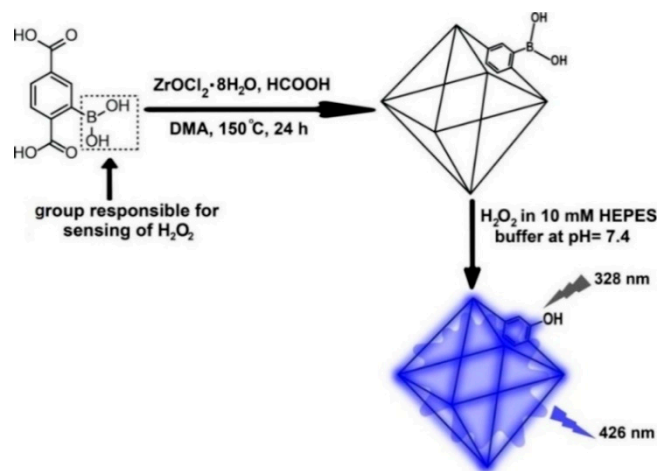


**Figure 6.** Synthesis of Zr-UiO-66-B(OH)<sub>2</sub> for the selective fluorescent detection of H<sub>2</sub>O<sub>2</sub> in HEPES buffer solutions. Reprinted with permission from [109]. Copyright (2018) American Chemical Society.

#### 4.1.5. Zr-MOFs for Optical pH Sensors

Owing to their excellent chemical stability in water within a wide pH range (as mentioned in Section 3), it is feasible to utilize Zr-MOFs in optical pH sensors. Since porphyrin-based linkers can show significant and reversible changes in both absorbance and fluorescence during the protonation and deprotonation processes, the water-stable porphyrinic Zr-MOFs are considered as attractive candidates for pH-dependent optical sensing. For example, in 2013, Zhou et al. first demonstrated the pH-dependent fluorescence of a mesoporous porphyrinic Zr-MOF, PCN-225 [113]. It was reported that the fluorescence emission peak of the MOF at around 725 nm can increase with increasing pH values from 0 to 10.2, and such an increase is much more remarkable when the pH is higher than 7. By utilizing the sensitive fluorescent response of such porphyrinic Zr-MOFs for pH sensing in weakly alkaline solutions, Lu et al. also demonstrated the incorporation of rhodamine B isothiocyanates, which possess the fluorescence that can sensitively respond to the pH in acidic solutions, into the MOF to design the dual-emitting pH sensor capable for a wide range of pH [114]. On the other hand, Li et al. first demonstrated the use of a porphyrinic Zr-MOF, PCN-222, for the colorimetric pH sensors in 2014 [115]. The porphyrin MOF was reported to show the reversible changes in color as well as fluorescent signal within the low pH range. Generally, for such a porphyrinic Zr-MOF, a sharp color change from purple to green can be observed when the pH value is reduced to 3, and the distinct color change can occur when the pH value further drops to pH 2 and lower (Figure 7). Very recently, Cabanillas-Gonzalez, Cunha-Silva, Pedrosa, and coworkers also utilized the reversible color change of porphyrinic Zr-MOFs during protonation/deprotonation in the colorimetric sensors for trifluoroacetic acid vapor [116]. In addition to the porphyrinic Zr-MOFs, the PSM of other optically active ligands into Zr-MOFs was also used to design the sensitive pH probes. For example, by incorporating carboxynaphthofluorescein into a Zr-MOF, NU-1000, the resulting material could be applied for colorimetric pH sensors [117], and by functionalizing indole moiety into UiO-66-NH<sub>2</sub>, the obtained material could be utilized in luminescent pH sensors [118].

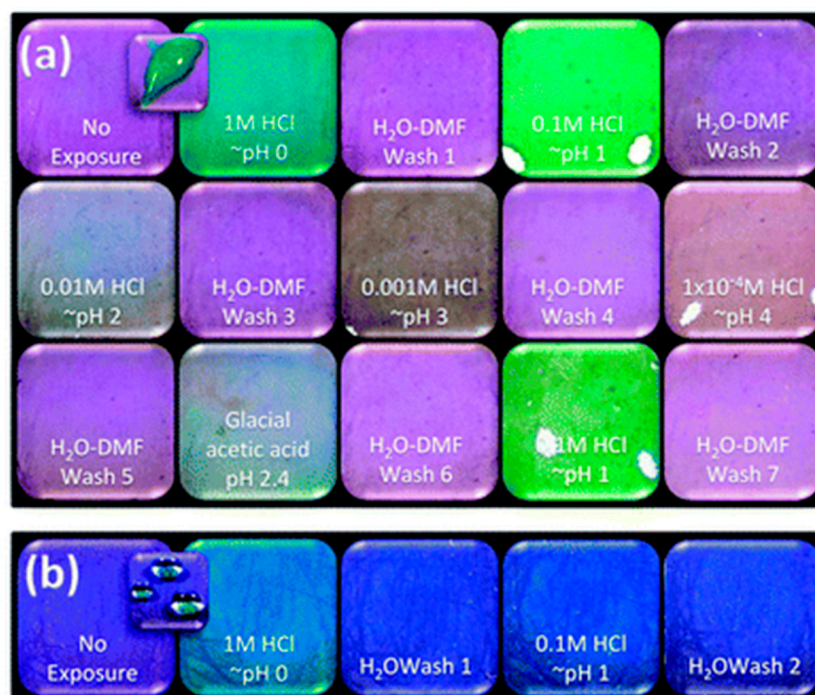


**Figure 7.** Photographs of the (a) PCN-222 and (b) porphyrinic linker taken under ambient light, after the exposure to various aqueous solutions and reversal washes between each exposure. Reprinted with permission from [115]. Copyright (2014) Royal Society of Chemistry.

#### 4.1.6. Hf-MOFs for Optical Sensors

As mentioned earlier, Hf-MOFs show similar structures and characteristics compared to Zr-MOFs. Owing to their excellent stability in water, the use of Hf-MOFs in optical sensors in aqueous solutions should be as feasible as Zr-MOFs, but the incorporation of optically active moieties within Hf-MOFs is also required, as the hafnium-based clusters themselves also show negligible absorbance and fluorescence in visible region. Reports on the use of Hf-MOFs for optical sensors are still rare so far, but it should be noted that from the application point of view, the advantages of Hf-MOFs compared to their Zr-based isostructural MOFs should be considered first before the use of Hf-MOFs for optical sensors. For example, as mentioned in Section 1, Hf-MOFs are in principle more chemically stable than Zr-MOFs and Ti-MOFs owing to their stronger metal-oxygen bonds. Thus, the use of Hf-MOFs may be highly desirable if some harsh sensing conditions that structurally damage Zr-MOFs and Ti-MOFs are required.

In 2018, Biswas et al. demonstrated the use of the boronic acid-functionalized UiO-66-type Hf-MOF (Hf-UiO-66-B(OH)<sub>2</sub>) for the turn-on luminescent detection of common reactive oxygen species (ONOO<sup>−</sup>) in neutral HEPES buffer solutions with a low detection limit of 9.0 nM [119]. The boronic groups reacted with ONOO<sup>−</sup> to form hydroxy-functionalized ligands via the oxidative cleavage reaction, which resulted in a turn-on fluorescence emission. The same research group also reported the turn-off fluorometric sensing of free chlorine and the turn-on fluorometric detection of the cyanide ions via utilizing the structurally distinct functionalized Hf-MOFs [120,121]. Another notable example was recently reported by Li, Lu, and coworkers, which demonstrated the use of a Hf-MOF constructed from H<sub>4</sub>BTTB (4,4',4'',4'''-(pyrazine-2,3,5,6-tetrayl)tetrabenzoic acid) linker, a well-known aggregation-induced-emission molecule, for the detection of Cr<sub>2</sub>O<sub>7</sub><sup>2−</sup> ions in water [122]. Furthermore, Li et al. demonstrated the use of a Hf-MOF constructed from the 4',4'',4'''-(4,4'-(1,4-phenylene)bis(pyridine-6,4,2-triyl))-tetrabenzoic acid linker for the self-calibrating ratiometric fluorescent detection of sulfonic derivative, which was the first example of replacing terminal H<sub>2</sub>O/OH<sup>−</sup> groups presented in the MOF structure by an analyte [123].

#### 4.1.7. Ti-MOFs for Optical Sensors

As mentioned in Section 1, Ti-MOFs in general possess quite distinct structures and topologies compared to Zr-MOFs and Hf-MOFs, but they are also chemically stable in water. Thus, some research efforts have also been made to design the Ti-MOFs constructed from or installed with optically active ligands for use in optical sensors, though the examples so far are still rare compared to those based on Zr-MOFs.

For example, in an early study reported by Qian et al. in 2016, nanosheets of a two-dimensional Ti-MOF constructed from the 2,5-dihydroxyterephthalic acid linker, NTU-9-NS, were synthesized and applied for the turn-off luminescent detection of Fe<sup>3+</sup> ions in water. The competitive absorption of light source and the interaction between the MOF linker and analyte were reported as the main reasons for such a quenching effect [124]. The similar luminescent detection of Fe<sup>3+</sup> ions by another Ti-MOF constructed from the 4,4',4''-tricarboxytriphenylamine linker, ZSTU-1, was also demonstrated by Guo, Xu, and coworkers in a recent work [125]. On the other hand, as reported by Kansal et al., the Lewis acid-base interaction between Cu<sup>2+</sup> ions and the amine groups of a common Ti-MOF, NH<sub>2</sub>-MIL-125(Ti), could be utilized in the turn-off luminescent detection of Cu<sup>2+</sup> ions [126]. In addition to ion sensors, two fluorogenic Ti-MOFs (ZSTU-1 and ZSTU-2) were also applied for the selective turn-off detection of picric acid (PA) against other nitroaromatic explosives in aqueous media [125,127]; the ZSTU-1 was even reported to show the optical sensing ability toward PA vapor. A recent study also reported the direct use of NH<sub>2</sub>-MIL-125(Ti) for detecting protein kinase A by means of the interaction between the phosphate groups and the MOF [128].

#### 4.1.8. Ce-MOFs for Optical Sensors

MOFs are constructed from Ce(IV)-based clusters as their nodes have been known to show a similar chemical stability in water compared to Zr-MOFs. Furthermore, the characteristics of these Ce-MOFs and their Zr-based isostructural analogs, such as the stability and catalytic activity, are highly tunable by adjusting the Zr-to-Ce ratio of the mix-metal nodes presented in the MOFs [51,129–131]. In addition, the presence of cerium within Ce-MOFs results in the Ce(III)/Ce(IV) redox activity of a part of the cerium sites that are uncoordinated with linkers. It should be noted that in principle, the complete reduction of all Ce(IV) atoms in a Ce-MOF to Ce(III) should result in structural degradation; careful characterizations of the Ce-MOF after the sensing operation are thus suggested. Owing to such redox activity and water stability, the design of Ce-MOFs with optically active moieties for sensing applications in aqueous environments should be of interest, and the resulting sensing performance may outperform the corresponding Zr-based isostructural MOFs for certain sensing purposes. However, reports on the use of Ce-MOFs for luminescent or colorimetric sensors are still rare so far.

An early example reported by Qian, Chen, and coworkers in 2017 showed that a Ce-MOF (ZJU-136-Ce) exhibits the turn-on fluorescence signal for the detection of ascorbic acid (AA). The redox reaction between the Ce(IV) sites and AA results in the turn-on fluorescence upon the exposure to the analyte (Figure 8) [132]. A very recent work also showed that the similar turn-on luminescent detection of AA could be achieved by two other structurally distinct Ce-MOFs [133]. On the other hand, the redox activity of Ce-MOFs could result in the inherent oxidase-like activity for sensing purposes. As demonstrated by Biswas, Dhakshinamoorthy, and coworkers, a UiO-66-type Ce-MOF constructed from the 3,4-dimethylthieno[2,3-b]thiophene-2,5-dicarboxylic acid linker could be utilized to oxidize 3,3',5,5'-tetramethylbenzidine (TMB) or 2,2'-azinobis(3-ethylbenzothiazoline-6-sulfonic acid) (AzBTS), which is known as the chromogenic peroxidase reagent [134]. As a result, such a Ce-MOF with a remarkable oxidase-mimic activity could be served as the colorimetric sensing platform for biothiols in acetate buffer solutions [134]. Another notable example was reported by Tan and coworkers, which showed that the catalytic activity for the oxidation of TMB occurring on a Ce-MOF can be inhibited by the addition of single-stranded DNA, and the catalytic activity can be partially recovered upon the exposure to Hg<sup>2+</sup> ions that bind to the DNA to generate the double-stranded DNA; the colorimetric sensor for Hg<sup>2+</sup> ions was thus established [135].

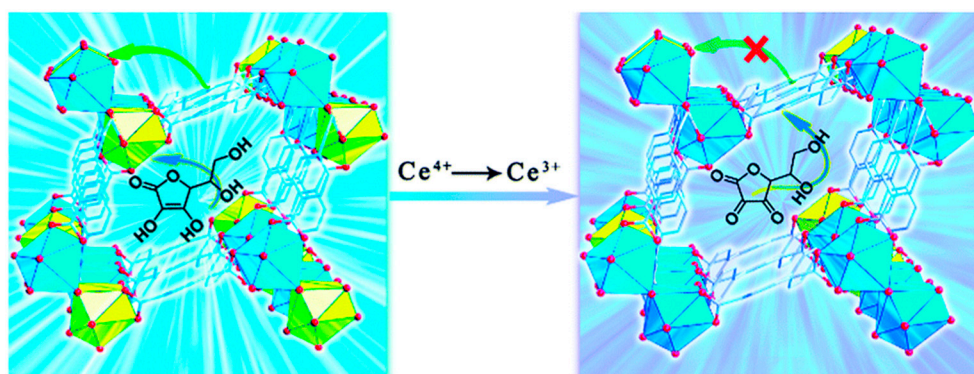


**Figure 8.** Schematic demonstration of a Ce-MOF, ZJU-136-Ce, for the luminescent detection of AA. Reprinted with permission from [132]. Copyright (2017) Royal Society of Chemistry.

#### 4.2. Electrochemical Sensors

Electrochemical sensors utilize the changes in potential, current, or resistance associated with the electrochemical reactions occurring on the electrode surface to determine the concentration of the targeted analyte [136]. Compared to the optical chemosensors, electrochemical sensors do not require spectroscopic instruments, which makes it easier to design the small and portable sensing systems. One of the most common commercially

available examples of electrochemical sensors are the glucose sensors [137,138]. A thin film of active material is usually coated on the surface of the electrode to further enhance the sensitivity or selectivity of the electrochemical sensor toward the specific targeted analyte [136]; such “modified electrodes” are commonly used in the design of electrode materials for electrochemical sensors [139]. Therefore, the use of MOFs and MOF-based materials as the modified thin films deposited on the electrode surfaces thus became appealing since the highly porous framework immobilized with spatially separated active sites in its pore is expected to further amplify the sensing signal [140]. For amperometric sensors, which belong to one common type of electrochemical sensors relying on the current response measured at a fixed applied potential, their sensing mechanisms usually consist of the electrocatalytic reactions involving the targeted analyte. Thus, the use of MOF-based electrocatalysts that are capable to selectively electrocatalyze the analyte is highly desirable [21,141,142]. Owing to these reasons, the applications of MOFs for electrochemical sensors have been widely reported since 2013 [141,142]. However, as most electrochemical sensors require the use of aqueous electrolytes, the direct use of less stable MOFs might result in the formation of MOF-derived metal oxides or hydroxides on the electrode surface during the electrochemical processes; the water-stable group 4 metal-based MOFs are thus more desirable for such purposes.

#### 4.2.1. Charge Transport in Group 4 Metal-Based MOFs

A key factor that needs to be considered first before the design of MOFs for electrochemical sensors is the charge transport within the selected MOFs [142]. As the electrochemical reactions only occur on the surface, for a porous thin film modified on an underlying electrode such as a MOF thin film incorporated with a high density of active sites, sufficient electronic conduction must be presented between these active sites within the MOF thin film in order to make the electrochemical reaction to occur on these active sites [143]. Thus, without considerable long-range charge transport within the MOF thin film, most active sites immobilized within the framework cannot be involved in the targeted electrochemical reaction. Unfortunately, almost all group 4 metal-based MOFs are electrically insulating [143,144], which makes it very difficult to properly utilize them in electrochemical sensors. Given that, there are several Zr-MOFs and Ti-MOFs that have been reported to show experimentally measurable and semiconductor-like band gaps, such band gaps usually reflect the band positions of the local structure. The long-range electronic conduction within the bulk material of such MOFs is still quite limited as the electrons are highly localized in such frameworks [145–147]. Except very limited examples that demonstrated the design and synthesis of electrically conductive Zr-MOFs [148–152], almost all the group 4 metal-based MOFs can only render charge transport via redox hopping in electrochemical systems [143]. The redox-hopping mechanism capable for long-range charge transport was commonly reported in redox-active polymeric thin films [139,153] and has been discovered in group 4 metal-based MOFs since 2013 [154]. With the redox-active units that possess a similar redox potential and are spatially separated with a close enough distance between each other, charge can be transported via the reversible redox reactions of these active units coupled with the adsorption/desorption of counter ions for charge neutralization under electrochemical operations [155–157]. By utilizing such redox-hopping pathways, electrochemically addressable MOF-based thin films with remarkable electrochemical responses can be obtained, even though the bulk MOF shows no intrinsic electrical conductivity [143]. As the nodes of Zr-MOFs and Hf-MOFs are redox innocent, the use of redox-active linkers or the post-synthetic incorporation of redox-active units on the nodes is necessary to render redox hopping in these MOFs. Several studies demonstrated by different research groups have shown the design and synthesis of redox-active Zr-MOFs possessing redox-hopping-based electrochemical activity [56,158–163]. Moreover, our recently published work also showed that the redox-hopping charge transport can be observed in a redox-active Ce-MOF with unsaturated hexa-cerium nodes presented in its structure [164]. The similar electrochemical activity of another structurally well-defined

cerium-based MOF was also reported by Öhrström et al. in a very recent work [165]. With sufficient charge transport between the active sites within these water-stable MOFs, such MOF thin films should be considered as attractive candidates for electrochemical sensing purposes.

#### 4.2.2. Progress in the Use of Group 4 Metal-Based MOFs for Electrochemical Sensors

As the redox-hopping charge transport was mainly reported for Zr-MOFs, compared to those for Hf-MOFs, Ti-MOFs, and Ce-MOFs, more research efforts have been made to utilize Zr-MOFs and related materials in electrochemical sensors. The first published example regarding the use of Zr-MOFs in electrochemical sensors was reported in our early work published in 2015 [166]. In this work, a Zr-MOF constructed from porphyrinic TCPP linkers, MOF-525 [49], was applied for electrochemical determination of nitrite in aqueous KCl solutions. As shown in Figure 9a, charge transport can be facilitated by redox hopping between the porphyrinic units presented within the MOF-525 thin film, and these porphyrinic moieties also play the role as the electrocatalyst to electrochemically catalyze the oxidation of nitrite, which results in the amperometric sensing response [166]. The use of various porphyrinic Zr-MOFs and their nanocomposites for electrochemical nitrite sensors was thereafter demonstrated in several studies [151,167–170]. As these Zr-MOFs with porphyrinic building blocks can render redox hopping to transport charge, and porphyrins also consist of common electrocatalysts capable for catalyzing various analytes or mediators, such porphyrinic Zr-MOFs have been utilized in electrochemical sensors for a range of analytes in addition to nitrite [171–180]. For example, in an early example published in 2015, Lei et al. demonstrated the use of another porphyrinic Zr-MOF, PCN-222, to electrocatalyze oxygen reduction in PBS [171]. The electrocatalytic process was further utilized as the electrochemical probe for DNA sensors. The similar electrocatalytic oxygen reduction occurring on various kinds of porphyrinic Zr-MOF-based materials was thereafter utilized to enhance the electrochemical sensing responses for biomolecules such as thrombin [177] and ochratoxin A [178]. One notable example was demonstrated by Zhang and coworkers in 2016, which applied PCN-222 for photoelectrochemical sensors for the first time [172]. In this work, the photoelectrochemical reduction of oxygen catalyzed by the porphyrinic Zr-MOF in the presence of dopamine was reported in HEPES buffer solutions, and the resulting photocurrent can be suppressed after further modifying  $\alpha$ -casein on the electrode surface; the label-free photoelectrochemical sensor for  $\alpha$ -casein was thus developed [172]. It should be noted that the HEPES buffer solution was used here instead of the commonly used PBS to ensure the structural integrity of the Zr-MOF [55]. A very recent work reported by Fischer, Li, and coworkers also suggested that the porphyrinic Zr-MOF thin films could be applied for the selectively electrochemical detection of nitrobenzene and their derivatives in NaCl solutions [180]. As the redox hopping-based charge transport within such porphyrinic Zr-MOFs is known to be less efficient [166], especially between different MOF crystals, the design of electrically conductive MOF-based nanocomposites with the nanocarbons or conducting polymers to facilitate the interparticle electron conduction can further enhance the sensing performances. Such porphyrinic Zr-MOF-based nanocomposites have been synthesized and utilized in the electrochemical detections for nitrite [167], dopamine [174], luteolin [175], and chloramphenicol [179] in various studies.

In addition to the redox-active porphyrinic Zr-MOFs, several Zr-MOFs constructed from redox-innocent linkers, such as UiO-66, MOF-801, and their composite materials, have been directly applied for the electrochemical sensors toward a range of analytes in PBS [181–190]. As mentioned previously, PBS may cause the structural degradation of Zr-MOFs to form MOF-derived materials [54,55], for fundamentally probing the electrochemical sensing behaviors of the original Zr-MOF with well-preserved porosity and crystallinity, the use of other buffered systems is necessary. However, the lack of charge-transport pathways within these redox-innocent and electrically insulating Zr-MOFs during the electrochemical operations then becomes the main concern. Functionalizing spatially dispersed redox-active sites within such a redox-inactive Zr-MOF by PSM is one of the so-

lutions to render the hopping-based charge transport during the electrochemical processes without forming MOF-derived materials. For example, in our recent work, a redox-active polyoxometalate,  $V_{10}O_{28}$ , was post-synthetically immobilized within the entire framework of a Zr-MOF, NU-902. As illustrated in Figure 9b, the charge hopping by means of the reversible redox reactions of  $V_{10}O_{28}$  was observed during the electrochemical operations in MOPS solutions, and the  $V_{10}O_{28}$  itself was found to act as the electrocatalyst for dopamine oxidation, which was applied for electrochemical dopamine sensors [191]. Similarly, the post-synthetic immobilization of spatially separated Ir(III)/Ir(IV) sites within defective UiO-66 can also render the hopping-based charge transport within this Zr-MOF, and the redox-active iridium sites were found to be capable to detect nitrite in aqueous perchlorate-based electrolytes electrochemically while maintaining the crystallinity of the MOF [192].

On the other hand, another strategy to utilize such structurally robust, porous, but redox-inactive Zr-MOFs for electrochemical sensors is to incorporate other catalytic and electrically conductive materials into the MOF pore. For example, in 2016, Zeng et al. demonstrated the immobilization of AuPd bimetallic nanoparticles within a Zr-MOF, UiO-66-NH<sub>2</sub>, and the resulting composite material can be used to electrochemically detect nitrite due to the presence of the electrocatalytic nanoparticles (Figure 9c) [193]. The electrochemical sensing experiments were conducted in acetate buffer solutions, where the structure of Zr-MOF can remain intact. Ma, Wang, and coworkers incorporated a conducting polymer, polyaniline, into UiO-66-NH<sub>2</sub> by performing the in-situ polymerization of aniline in the presence of MOF crystals, and the Zr-MOF-polymer composite material was applied for electrochemical cadmium ion detection in acetate buffer solutions [194]. A recent study from our group also showed that by electrodepositing metallic cobalt within the pore of thin films of a redox-innocent Zr-MOF, the resulting continuous and pore-confined cobalt can exhibit the electrochemical sensing activity toward H<sub>2</sub>O<sub>2</sub> in the MOPS buffer solutions and outperform the flat cobalt electrodeposited in the absence of Zr-MOF [195].

In an early study demonstrated by Hu et al., the modified electrode of NH<sub>2</sub>-MIL-125(Ti) was reported to show the photoelectrochemical activity to oxidize Mn<sup>2+</sup> and was applied for the determination of Mn<sup>2+</sup> in tea samples (see Figure 9d) [196]. The same research group also showed that such a Ti-based MOF can be utilized in the photoelectrochemical detection of clethodim [197]. However, published examples of structurally well-defined Ti-MOFs applied for electrochemical sensors are still quite rare.

Owing to the potential redox activity of their metal-based nodes, Ce-based MOFs have attracted attention for their use in electrochemical sensors in a few studies published recently. Though this is beyond the scope of group 4 metal-based MOFs, the Ce(III)-based MOF, which was synthesized from the Ce(III) precursor, was reported for the use in electrochemical determinations of telomerase [198] and bisphenol A [199], respectively. Very recently, Zhu and coworkers also synthesized a nanocomposite composed of such a cerium-based MOF and carbon nanotubes that is capable of the simultaneous detection of hydroquinone and catechol in PBS [200]. However, the water-stable Ce(IV)-based MOFs with well-defined structures, such as Ce-UiO-66 and Ce-MOF-808, have not been reported for electrochemical sensors yet.

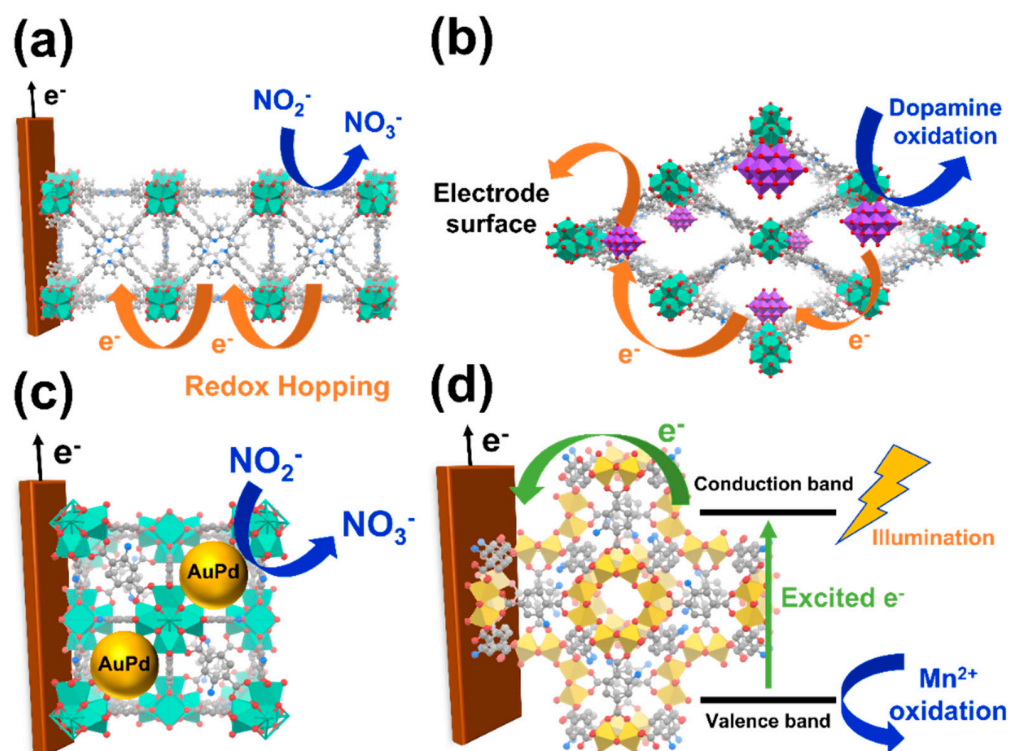


**Figure 9.** (a) The use of a redox-active porphyrinic Zr-MOF, MOF-525, to render hopping-based charge transport and electrochemically detect nitrite [166–168]. (b) Immobilization of  $\text{V}_{10}\text{O}_{28}$  clusters within a Zr-MOF, NU-902, to render both the charge transport and the electrocatalytic activity for dopamine detection [191]. (c) AuPd nanoparticles immobilized within UiO-66-NH<sub>2</sub> for electrochemical nitrite detection [193]. (d) Photoelectrochemical detection of  $\text{Mn}^{2+}$  ions by utilizing a Ti-MOF, NH<sub>2</sub>-MIL-125(Ti), as the catalytic thin films [196]. Elemental colors used in the MOF structures: cyan—Zr; yellow—Ti; purple—V; red—O; blue—N; grey—C; white—H.

#### 4.3. Chemiresistive Sensors and Others

The chemiresistive sensors rely on the change in the resistance of the active material upon the exposure to the targeted analyte as the sensing signal; such sensors are more frequently utilized to determine the concentrations of toxic gases or the relative humidity in gaseous environments [201,202]. As a decent electrical conductivity is needed, semiconducting inorganic metal oxides, conducting polymers, and carbon-based materials are usually utilized as the active materials in such sensors [201–203]. Research efforts have been made to design various electrically conductive MOFs as well as MOF-derived materials for the use in chemiresistive sensors, which can be found in some recently published review articles [204,205]. As mentioned in detail in Section 4.2.1, since almost all group 4 metal-based MOFs are electrically insulating without the presence of electrolytes and applied potential, examples of such MOFs for chemiresistive sensors relying on electronic conduction in MOFs are relatively rare. Without designing the electrically conductive group 4 metal-based MOFs, the role of such MOFs in the application of most resistive sensors usually belongs to the additive to enhance the sensing performances of another active material. However, it should be noted that since some Zr-MOFs have been known to show decent proton conductivity under a high relative humidity [206], the use of such group 4 metal-based MOFs in resistive or capacitive humidity sensors may be feasible, as investigated in one early work published by Ruan, Wen, and coworkers [207].

For chemiresistive gas sensors relying on the electronic conduction occurring in these group 4 metal-based MOFs, the first example was demonstrated by Hupp et al. [208]. The continuous one-dimensional (1D) strands of tin oxide were post-synthetically deposited within the 1D mesoporous channels of a Zr-MOF, NU-1000, by a self-limiting

solvothermal installation in MOFs (SIM) technique. As a result, the electrical insulating Zr-MOF can show moderate electrical conductivity after the deposition of tin oxide strands, and the resulting material, named as “Sn-SIM (3 cycles)”, was found to exhibit a significant and reversible change in electrical conductance upon the exposure to the reductive hydrogen gas at room temperature (Figure 10a) [208]. Another example regarding the Zr-MOF-based chemiresistive sensors for hydrogen gas was recently reported by Doan and coworkers [209]. In this work, Pd nanoparticles were post-synthetically installed within the pore of a Zr-MOF, and it was found that the Pd@Zr-MOF can be served as the active material for the chemiresistive hydrogen sensor operated at 150 °C with a remarkable selectivity against other common volatile organic compounds. In addition, Kalidindi et al. reported that UiO-66 and its derivatives can be applied for chemiresistive sensors toward SO<sub>2</sub>, NO<sub>2</sub>, and CO<sub>2</sub> gases at an operating temperature of 150 °C, though the resistive responses of such Zr-MOFs are still within the range of 10<sup>-10</sup> Ohm owing to the low electrical conductivities of these Zr-MOFs [210]. Utilizing MOFs as the additive to composite with the active sensing material may also improve the performances for chemiresistive sensors. For example, mixing UiO-66 crystals with graphene can suppress the resistive sensing responses of the pristine graphene for methanol and ethanol and significantly enhance the response for chloroform gas. Such a Zr-MOF-graphene composite was thus applied for the selective chemiresistive sensor toward chloroform, as reported by Losic and coworkers [211]. In addition to the chemiresistive sensors, another notable example was recently demonstrated by Simchi et al., which is the first study reporting the use of Zr-MOF in piezoelectric sensors [212]. As shown in Figure 10b, UiO-66 was added during the electrospinning fabrication of poly(vinylidene fluoride) (PVDF) nanofibrous membrane to prepare the MOF-PVDF composite membrane, and it was found that the crystallinity of the polymer can be obviously increased with the MOF additive, which results in the better piezoelectric sensing performance of PVDF for arterial pulse monitoring. It is worth noting that all the aforementioned examples are based on Zr-MOFs; the use of Ti-MOFs or Ce-MOFs for chemiresistive sensors or piezoelectric sensors has not been reported yet.

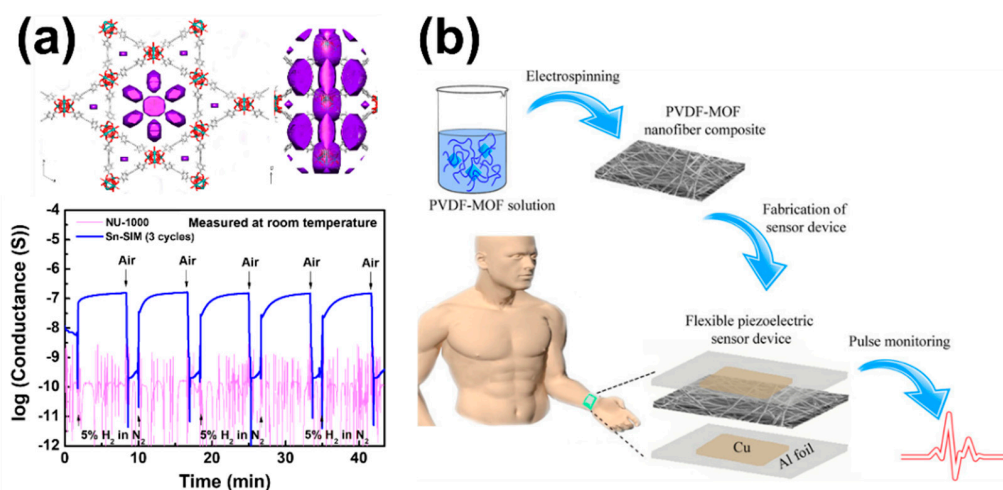


**Figure 10.** (a) (top) Electron density map of 1D tin oxide strands (shown in purple color) deposited within the hexagonal mesoporous channels of NU-1000; (bottom) chemiresistive hydrogen sensor operated at room temperature with the use of the Sn-SIM (3 cycles) material. Adapted with permission from [208]. Copyright (2018) American Chemical Society. (b) The addition of Zr-MOF (UiO-66) into PVDF membrane to enhance the piezoelectric sensing performance for arterial pulse monitoring. Reprinted with permission from [212]. Copyright (2020) American Chemical Society.

## 5. Future Outlooks

We have discussed the recent progress in the use of group 4 metal-based MOFs and related materials for various sensing systems such as optical sensors, electrochemical sensors, chemiresistive sensors, and other sensors for a range of analytes. Since these MOFs

possess remarkable chemical stability in a range of aqueous solutions, and their relatively large pore sizes and high structural diversity can allow various kinds of PSM to build the spatially accessible active sites with a high density, there are lots of opportunities in the applications of such group 4 metal-based MOFs for chemical sensing purposes. In addition to utilizing the active moieties for sensing purposes as the building blocks to synthesize the MOF structures, the uncoordinated metal-based clusters or defect sites presented within these MOFs can also allow the incorporation of active sites for sensing via PSM, which further increases the possibility to design materials for specific targets. Even though these MOFs are in general considered as the stable MOFs in water, the presence of strong alkaline solutions or strongly coordinated ions with a high concentration may still cause the structural degradation of these MOFs. Thus, the chemical stability of these MOFs during the sensing operations still needs to be considered with care, especially for the analytical systems operated in buffer solutions, which are quite common in biosensing applications. As the systematic studies regarding the chemical stability of various Zr-MOFs, Ti-MOFs, Hf-MOFs, and Ce-MOFs in a range of common buffer solutions are still rare so far, structural characterizations of the MOF after the sensing experiments may be necessary to gauge the structural integrity of the MOF for a new chemical sensing process.

A range of material-design strategies have been utilized to synthesize the optically active group 4 metal-based MOFs for fluorescent and colorimetric detection of various analytes. Given such optical sensing processes do not require long-range transport of electrons within the bulk material, the highly porous and interconnected pore structures of such MOFs incorporated with spatially separated optically active moieties provide the obvious benefits for achieving the sensitive and fast optical responses. With the rational selection of chemical functional groups presented within the entire framework, the resulting group 4 metal-based MOFs should be the potential platforms for the sensitive and selective optical detections of specific analytes including ions, organic compounds, and inorganic small molecules in aqueous solutions. For the optical detection of biomolecules and some drug molecules, the size of the targeted analyte compared to the pore size of the MOF should be considered to ensure the accessibility of the analyte to the internal active sites presented within the framework. As the pore size of such group 4 metal-based MOFs is highly tunable from less than 1 nm to more than 5 nm, pore size of the MOF should play an important role in certain chemical sensing processes. The selectivity may be affected if the pore size of the selected MOF can exclude the penetration of the interferents with large molecular sizes.

Unlike optical sensors, electrochemical sensors based on MOFs face a serious obstacle due to the poor electrical conductivity of most MOFs. The use of MOF-derived carbon or metal oxides for electrochemical sensors can effectively resolve this issue, but such materials lose the regular porosity and tunable intra-framework chemical functionality, which is the main fantastic characteristics of MOFs for sensing applications. As the existed group 4 metal-based MOFs with intrinsic electrical conductivity are still very rare in literature, utilizing redox hopping-based pathways to transport charge within the intrinsically insulating framework during the electrochemical sensing processes is more feasible. Such electrochemically active and water-stable MOFs can be synthesized by using the redox-active ligand as the linker during MOF synthesis, installing the redox-active sites in the MOF via PSM, or incorporating another conducting material with a continuous phase within the pore of the MOF. It should be noted that utilizing the MOF with a high intrinsic electrical conductivity may not always be beneficial for electrochemical sensing purposes, as the highly porous and electrically conductive MOF should provide a huge non-Faradaic current, which is considered as the background signal for amperometric sensors and is not desirable for achieving low limits of detection. The group 4 metal-based MOFs relying on the redox hopping-based charge transport are thus advantageous for such electroanalytical purposes, since such MOFs show negligible current response without applying the potential that initiates the Faradaic reaction.

For resistive and capacitive sensors, the direct use of group 4 metal-based MOFs is even more challenging compared to the electrochemical sensors, as a high electrical conductivity upon the adsorption or desorption of the analyte is usually required. However, more opportunities may be there for the use of such MOFs as the additive during the fabrication of another active sensing material. As mentioned in the previous section, a recent study suggested that the addition of a minor amount of Zr-MOF into the polymer membrane can enhance the crystallinity of the polymer, which can thus improve the piezoelectric sensing performance of the polymer. These chemically robust group 4 metal-based MOFs may play the similar role in other sensing systems in future studies.

Moreover, the next generation of sensors often requires flexibility and conformability without compromising performance [213]. The stability of group 4 metal-based MOFs may provide high compatibility to a wide range of stretchable or conducting polymers to prepare wearables sensors. In addition, the geometrical design of sensors, such as surface roughness and hierarchical structures, can impart enhanced sensitivity and functionality [214]. The fabrication of these highly complex devices can be achieved by advanced processing techniques such as additive manufacturing. Some recent reports have attempted to incorporate MOFs into additive manufacturing [215–217]. However, more work is needed to fully explore the emerging properties from the combination of MOFs and additive manufacturing. The potentials of group 4 metal-based MOFs can be further expanded by utilizing their stability and activity in preparing high-performance composite materials. Within such composite materials aiming for sensors, the rigid and highly porous MOF crystals may play dual roles as the active sites for chemical sensing as well as the additive or filler to further enhance certain properties of the polymer matrix.

It should be noted that most published examples reporting the use of group 4 metal-based MOFs in chemical sensors so far only focused on Zr-MOFs. Even though the chemical stability of Ti-MOFs, Hf-MOFs, and Ce-MOFs is in general comparable to that of Zr-MOFs, studies on the use of such MOFs in chemosensors are still relatively rare. Enormous opportunities are thus there for the use of these MOFs in chemosensors. Especially, Ce-MOFs possessing water stability, structural diversity, as well as redox activity may be an attractive platform for a range of chemical sensing purposes. In short, the appropriate design of MOFs-based materials may develop the sensitive and selective chemical sensors for practical applications such as medical diagnosis and environmental monitoring.

**Author Contributions:** S.P. carried out the conceptualization, formal analysis, investigation, and writing—original draft. S.-S.Y. contributed to the resources, writing—original draft, writing—review & editing, supervision, project administration, and funding acquisition. C.-W.K. was involved with the conceptualization, resources, writing—review & editing, supervision, and funding acquisition. All authors have read and agreed to the published version of the manuscript.

**Funding:** We thank the funding support from Ministry of Science and Technology (MOST) of Taiwan under the project number 110-2221-E-006-017-MY3. This article was also supported by Higher Education Sprout Project, MOE, Taiwan to the Headquarters of University Advancement at National Cheng Kung University (NCKU).

**Institutional Review Board Statement:** Not applicable.

**Informed Consent Statement:** Not applicable.

**Data Availability Statement:** Not applicable.

**Conflicts of Interest:** The authors declare no conflict of interest.

## References

1. Kreno, L.E.; Leong, K.; Farha, O.K.; Allendorf, M.; Van Duyne, R.P.; Hupp, J.T. Metal–Organic Framework Materials as Chemical Sensors. *Chem. Rev.* **2012**, *112*, 1105–1125. [[CrossRef](#)]
2. Zhang, H.; Xiong, P.; Li, G.; Liao, C.; Jiang, G. Applications of multifunctional zirconium-based metal-organic frameworks in analytical chemistry: Overview and perspectives. *TrAC Trends Anal. Chem.* **2020**, *131*, 116015. [[CrossRef](#)]

3. Olorunyomi, J.F.; Geh, S.T.; Caruso, R.A.; Doherty, C.M. Metal–organic frameworks for chemical sensing devices. *Mater. Horiz.* **2021**, *8*, 2387–2419. [[CrossRef](#)]
4. Furukawa, H.; Cordova, K.E.; O’Keeffe, M.; Yaghi, O.M. The Chemistry and Applications of Metal–Organic Frameworks. *Science* **2013**, *341*, 1230444. [[CrossRef](#)]
5. Kitagawa, S.; Kitaura, R.; Noro, S.-I. Functional Porous Coordination Polymers. *Angew. Chem. Int. Ed.* **2004**, *43*, 2334–2375. [[CrossRef](#)]
6. Ferey, G. Hybrid porous solids: Past, present, future. *Chem. Soc. Rev.* **2008**, *37*, 191–214. [[CrossRef](#)] [[PubMed](#)]
7. Murray, L.J.; Dincă, M.; Long, J.R. Hydrogen storage in metal–organic frameworks. *Chem. Soc. Rev.* **2009**, *38*, 1294–1314. [[CrossRef](#)]
8. He, Y.; Zhou, W.; Qian, G.; Chen, B. Methane storage in metal–organic frameworks. *Chem. Soc. Rev.* **2014**, *43*, 5657–5678. [[CrossRef](#)] [[PubMed](#)]
9. Li, J.-R.; Sculley, J.; Zhou, H.-C. Metal–Organic Frameworks for Separations. *Chem. Rev.* **2012**, *112*, 869–932. [[CrossRef](#)]
10. Herm, Z.R.; Bloch, E.D.; Long, J.R. Hydrocarbon Separations in Metal–Organic Frameworks. *Chem. Mater.* **2014**, *26*, 323–338. [[CrossRef](#)]
11. Lee, J.; Farha, O.K.; Roberts, J.; Scheidt, K.A.; Nguyen, S.T.; Hupp, J.T. Metal–organic framework materials as catalysts. *Chem. Soc. Rev.* **2009**, *38*, 1450–1459. [[CrossRef](#)]
12. Ma, L.; Abney, C.; Lin, W. Enantioselective catalysis with homochiral metal–organic frameworks. *Chem. Soc. Rev.* **2009**, *38*, 1248–1256. [[CrossRef](#)]
13. Yang, Q.; Xu, Q.; Jiang, H.-L. Metal–organic frameworks meet metal nanoparticles: Synergistic effect for enhanced catalysis. *Chem. Soc. Rev.* **2017**, *46*, 4774–4808. [[CrossRef](#)] [[PubMed](#)]
14. Konnerth, H.; Matsagar, B.M.; Chen, S.S.; Precht, M.H.G.; Shieh, F.-K.; Wu, K.C.W. Metal–organic framework (MOF)-derived catalysts for fine chemical production. *Coord. Chem. Rev.* **2020**, *416*, 213319. [[CrossRef](#)]
15. Torad, N.L.; Li, Y.; Ishihara, S.; Ariga, K.; Kamachi, Y.; Lian, H.-Y.; Hamoudi, H.; Sakka, Y.; Chaikittisilp, W.; Wu, K.C.W.; et al. MOF-derived Nanoporous Carbon as Intracellular Drug Delivery Carriers. *Chem. Lett.* **2014**, *43*, 717–719. [[CrossRef](#)]
16. Wu, M.X.; Yang, Y.W. Metal–organic framework (MOF)-based drug/cargo delivery and cancer therapy. *Adv. Mater.* **2017**, *29*, 1606134. [[CrossRef](#)]
17. Choi, K.M.; Jeong, H.M.; Park, J.H.; Zhang, Y.-B.; Kang, J.K.; Yaghi, O.M. Supercapacitors of Nanocrystalline Metal–Organic Frameworks. *ACS Nano* **2014**, *8*, 7451–7457. [[CrossRef](#)] [[PubMed](#)]
18. Sheberla, D.; Bachman, J.C.; Elias, J.S.; Sun, C.-J.; Shao-Horn, Y.; Dincă, M. Conductive MOF electrodes for stable supercapacitors with high areal capacitance. *Nat. Mater.* **2016**, *16*, 220–224. [[CrossRef](#)] [[PubMed](#)]
19. Wang, C.; Kaneti, Y.V.; Bando, Y.; Lin, J.; Liu, C.; Li, J.; Yamauchi, Y. Metal–organic framework-derived one-dimensional porous or hollow carbon-based nanofibers for energy storage and conversion. *Mater. Horiz.* **2018**, *5*, 394–407. [[CrossRef](#)]
20. Majewski, M.B.; Peters, A.W.; Wasielewski, M.R.; Hupp, J.T.; Farha, O.K. Metal–Organic Frameworks as Platform Materials for Solar Fuels Catalysis. *ACS Energy Lett.* **2018**, *3*, 598–611. [[CrossRef](#)]
21. Li, J.-H.; Wang, Y.-S.; Chen, Y.-C.; Kung, C.-W. Metal–Organic Frameworks Toward Electrocatalytic Applications. *Appl. Sci.* **2019**, *9*, 2427. [[CrossRef](#)]
22. Stassen, I.; Burtch, N.; Talin, A.; Falcaro, P.; Allendorf, M.; Ameloot, R. An updated roadmap for the integration of metal–organic frameworks with electronic devices and chemical sensors. *Chem. Soc. Rev.* **2017**, *46*, 3185–3241. [[CrossRef](#)]
23. Calvo, J.J.; Angel, S.M.; So, M.C. Charge transport in metal–organic frameworks for electronics applications. *APL Mater.* **2020**, *8*, 050901. [[CrossRef](#)]
24. Cohen, S.M. Postsynthetic Methods for the Functionalization of Metal–Organic Frameworks. *Chem. Rev.* **2012**, *112*, 970–1000. [[CrossRef](#)]
25. Islamoglu, T.; Goswami, S.; Li, Z.; Howarth, A.J.; Farha, O.K.; Hupp, J.T. Postsynthetic Tuning of Metal–Organic Frameworks for Targeted Applications. *Acc. Chem. Res.* **2017**, *50*, 805–813. [[CrossRef](#)]
26. Burtch, N.C.; Jasuja, H.; Walton, K.S. Water Stability and Adsorption in Metal–Organic Frameworks. *Chem. Rev.* **2014**, *114*, 10575–10612. [[CrossRef](#)] [[PubMed](#)]
27. Howarth, A.J.; Liu, Y.; Li, P.; Li, Z.; Wang, T.C.; Hupp, J.T.; Farha, O.K. Chemical, thermal and mechanical stabilities of metal–organic frameworks. *Nat. Rev. Mater.* **2016**, *1*, 15018. [[CrossRef](#)]
28. Yuan, S.; Qin, J.-S.; Lollar, C.T.; Zhou, H.-C. Stable Metal–Organic Frameworks with Group 4 Metals: Current Status and Trends. *ACS Cent. Sci.* **2018**, *4*, 440–450. [[CrossRef](#)] [[PubMed](#)]
29. Yuan, S.; Feng, L.; Wang, K.; Pang, J.; Bosch, M.; Lollar, C.; Sun, Y.; Qin, J.; Yang, X.; Zhang, P.; et al. Stable Metal–Organic Frameworks: Design, Synthesis, and Applications. *Adv. Mater.* **2018**, *30*, 1704303. [[CrossRef](#)] [[PubMed](#)]
30. Hu, Z.; Wang, Y.; Zhao, D. The chemistry and applications of hafnium and cerium(IV) metal–organic frameworks. *Chem. Soc. Rev.* **2021**, *50*, 4629–4683. [[CrossRef](#)] [[PubMed](#)]
31. Cavka, J.H.; Jakobsen, S.; Olsbye, U.; Guillou, N.; Lamberti, C.; Bordiga, S.; Lillerud, K.P. A New Zirconium Inorganic Building Brick Forming Metal Organic Frameworks with Exceptional Stability. *J. Am. Chem. Soc.* **2008**, *130*, 13850–13851. [[CrossRef](#)]
32. Chen, Z.; Hanna, S.L.; Redfern, L.R.; Alezi, D.; Islamoglu, T.; Farha, O.K. Reticular chemistry in the rational synthesis of functional zirconium cluster-based MOFs. *Coord. Chem. Rev.* **2019**, *386*, 32–49. [[CrossRef](#)]
33. Bon, V.; Senkovska, I.; Baburin, I.A.; Kaskel, S. Zr- and Hf-Based Metal–Organic Frameworks: Tracking Down the Polymorphism. *Cryst. Growth Des.* **2013**, *13*, 1231–1237. [[CrossRef](#)]

34. Dan-Hardi, M.; Serre, C.; Frot, T.; Rozes, L.; Maurin, G.; Sanchez, C.; Férey, G. A New Photoactive Crystalline Highly Porous Titanium(IV) Dicarboxylate. *J. Am. Chem. Soc.* **2009**, *131*, 10857–10859. [[CrossRef](#)]
35. Lammert, M.; Wharmby, M.T.; Smolders, S.; Bueken, B.; Lieb, A.; Lomachenko, K.A.; Vos, D.D.; Stock, N. Cerium-based metal organic frameworks with UiO-66 architecture: Synthesis, properties and redox catalytic activity. *Chem. Commun.* **2015**, *51*, 12578–12581. [[CrossRef](#)] [[PubMed](#)]
36. Jacobsen, J.; Ienco, A.; D'Amato, R.; Costantino, F.; Stock, N. The chemistry of Ce-based metal–organic frameworks. *Dalton Trans.* **2020**, *49*, 16551–16586. [[CrossRef](#)] [[PubMed](#)]
37. Lammert, M.; Glißmann, C.; Reinsch, H.; Stock, N. Synthesis and Characterization of New Ce(IV)-MOFs Exhibiting Various Framework Topologies. *Cryst. Growth Des.* **2017**, *17*, 1125–1131. [[CrossRef](#)]
38. Waitschat, S.; Fröhlich, D.; Reinsch, H.; Terraschke, H.; Lomachenko, K.A.; Lamberti, C.; Kummer, H.; Helling, T.; Baumgartner, M.; Henninger, S.; et al. Synthesis of M-UiO-66 (M = Zr, Ce or Hf) employing 2,5-pyridinedicarboxylic acid as a linker: Defect chemistry, framework hydrophilisation and sorption properties. *Dalton Trans.* **2018**, *47*, 1062–1070. [[CrossRef](#)]
39. Dodson, R.A.; Wong-Foy, A.G.; Matzger, A.J. The Metal–Organic Framework Collapse Continuum: Insights from Two-Dimensional Powder X-ray Diffraction. *Chem. Mater.* **2018**, *30*, 6559–6565. [[CrossRef](#)]
40. Howarth, A.J.; Peters, A.W.; Vermeulen, N.A.; Wang, T.C.; Hupp, J.T.; Farha, O.K. Best Practices for the Synthesis, Activation, and Characterization of Metal–Organic Frameworks. *Chem. Mater.* **2017**, *29*, 26–39. [[CrossRef](#)]
41. Düren, T.; Millange, F.; Férey, G.; Walton, K.S.; Snurr, R.Q. Calculating Geometric Surface Areas as a Characterization Tool for Metal–Organic Frameworks. *J. Phys. Chem. C* **2007**, *111*, 15350–15356. [[CrossRef](#)]
42. Zheng, W.; Liu, M.; Lee, L.Y.S. Electrochemical Instability of Metal–Organic Frameworks: In Situ Spectroelectrochemical Investigation of the Real Active Sites. *ACS Catal.* **2020**, *10*, 81–92. [[CrossRef](#)]
43. Miles, D.O.; Jiang, D.; Burrows, A.D.; Halls, J.E.; Marken, F. Conformal transformation of [Co(bdc)(DMF)] (Co-MOF-71, bdc = 1,4-benzenedicarboxylate, DMF = N,N-dimethylformamide) into porous electrochemically active cobalt hydroxide. *Electrochem. Commun.* **2013**, *27*, 9–13. [[CrossRef](#)]
44. Qu, C.; Jiao, Y.; Zhao, B.; Chen, D.; Zou, R.; Walton, K.S.; Liu, M. Nickel-based pillared MOFs for high-performance supercapacitors: Design, synthesis and stability study. *Nano Energy* **2016**, *26*, 66–73. [[CrossRef](#)]
45. Babu, K.F.; Kulandainathan, M.A.; Katsounaros, I.; Rassaei, L.; Burrows, A.D.; Raithby, P.R.; Marken, F. Electrocatalytic activity of Basolite™ F300 metal-organic-framework structures. *Electrochem. Commun.* **2010**, *12*, 632–635. [[CrossRef](#)]
46. Kandiah, M.; Nilsen, M.H.; Usseglio, S.; Jakobsen, S.; Olsbye, U.; Tilsted, M.; Larabi, C.; Quadrelli, E.A.; Bonino, F.; Lillerud, K.P. Synthesis and Stability of Tagged UiO-66 Zr-MOFs. *Chem. Mater.* **2010**, *22*, 6632–6640. [[CrossRef](#)]
47. Furukawa, H.; Gándara, F.; Zhang, Y.-B.; Jiang, J.; Queen, W.L.; Hudson, M.R.; Yaghi, O.M. Water Adsorption in Porous Metal–Organic Frameworks and Related Materials. *J. Am. Chem. Soc.* **2014**, *136*, 4369–4381. [[CrossRef](#)]
48. Feng, D.; Gu, Z.-Y.; Li, J.-R.; Jiang, H.-L.; Wei, Z.; Zhou, H.-C. Zirconium-Metalloporphyrin PCN-222: Mesoporous Metal–Organic Frameworks with Ultrahigh Stability as Biomimetic Catalysts. *Angew. Chem. Int. Ed.* **2012**, *51*, 10307–10310. [[CrossRef](#)] [[PubMed](#)]
49. Morris, W.; Voloskiy, B.; Demir, S.; Gándara, F.; McGrier, P.L.; Furukawa, H.; Cascio, D.; Stoddart, J.F.; Yaghi, O.M. Synthesis, Structure, and Metalation of Two New Highly Porous Zirconium Metal–Organic Frameworks. *Inorg. Chem.* **2012**, *51*, 6443–6445. [[CrossRef](#)]
50. Mondloch, J.E.; Bury, W.; Fairen-Jimenez, D.; Kwon, S.; DeMarco, E.J.; Weston, M.H.; Sarjeant, A.A.; Nguyen, S.T.; Stair, P.C.; Snurr, R.Q.; et al. Vapor-Phase Metalation by Atomic Layer Deposition in a Metal–Organic Framework. *J. Am. Chem. Soc.* **2013**, *135*, 10294–10297. [[CrossRef](#)] [[PubMed](#)]
51. Lammert, M.; Glißmann, C.; Stock, N. Tuning the stability of bimetallic Ce(IV)/Zr(IV)-based MOFs with UiO-66 and MOF-808 structures. *Dalton Trans.* **2017**, *46*, 2425–2429. [[CrossRef](#)]
52. Peters, A.W.; Li, Z.; Farha, O.K.; Hupp, J.T. Atomically Precise Growth of Catalytically Active Cobalt Sulfide on Flat Surfaces and within a Metal–Organic Framework via Atomic Layer Deposition. *ACS Nano* **2015**, *9*, 8484–8490. [[CrossRef](#)]
53. Noh, H.; Kung, C.-W.; Otake, K.-i.; Peters, A.W.; Li, Z.; Liao, Y.; Gong, X.; Farha, O.K.; Hupp, J.T. Redox-Mediator-Assisted Electrocatalytic Hydrogen Evolution from Water by a Molybdenum Sulfide-Functionalized Metal–Organic Framework. *ACS Catal.* **2018**, *8*, 9848–9858. [[CrossRef](#)]
54. Chen, Y.; Li, P.; Modica, J.A.; Drout, R.J.; Farha, O.K. Acid-Resistant Mesoporous Metal–Organic Framework toward Oral Insulin Delivery: Protein Encapsulation, Protection, and Release. *J. Am. Chem. Soc.* **2018**, *140*, 5678–5681. [[CrossRef](#)]
55. Bůžek, D.; Adamec, S.; Lang, K.; Demel, J. Metal–organic frameworks vs. buffers: Case study of UiO-66 stability. *Inorg. Chem. Front.* **2021**, *8*, 720–734. [[CrossRef](#)]
56. Lin, S.; Pineda-Galvan, Y.; Maza, W.A.; Epley, C.C.; Zhu, J.; Kessinger, M.C.; Pushkar, Y.; Morris, A.J. Electrochemical Water Oxidation by a Catalyst-Modified Metal–Organic Framework Thin Film. *ChemSusChem* **2017**, *10*, 514–522. [[CrossRef](#)]
57. Li, J.-H.; Chen, Y.-C.; Wang, Y.-S.; Ho, W.H.; Gu, Y.-J.; Chuang, C.-H.; Song, Y.-D.; Kung, C.-W. Electrochemical Evolution of Pore-Confined Metallic Molybdenum in a Metal–Organic Framework (MOF) for All-MOF-Based Pseudocapacitors. *ACS Appl. Energy Mater.* **2020**, *3*, 6258–6267. [[CrossRef](#)]
58. McDonagh, C.; Burke, C.S.; MacCraith, B.D. Optical Chemical Sensors. *Chem. Rev.* **2008**, *108*, 400–422. [[CrossRef](#)]
59. Hu, Z.; Deibert, B.J.; Li, J. Luminescent metal–organic frameworks for chemical sensing and explosive detection. *Chem. Soc. Rev.* **2014**, *43*, 5815–5840. [[CrossRef](#)]

60. Allendorf, M.D.; Bauer, C.A.; Bhakta, R.K.; Houk, R.J.T. Luminescent metal–organic frameworks. *Chem. Soc. Rev.* **2009**, *38*, 1330–1352. [[CrossRef](#)] [[PubMed](#)]
61. Hao, Y.; Chen, S.; Zhou, Y.; Zhang, Y.; Xu, M. Recent Progress in Metal–Organic Framework (MOF) Based Luminescent Chemodosimeters. *Nanomaterials* **2019**, *9*, 974. [[CrossRef](#)] [[PubMed](#)]
62. He, T.; Zhang, Y.-Z.; Kong, X.-J.; Yu, J.; Lv, X.-L.; Wu, Y.; Guo, Z.-J.; Li, J.-R. Zr(IV)-Based Metal-Organic Framework with T-Shaped Ligand: Unique Structure, High Stability, Selective Detection, and Rapid Adsorption of  $\text{Cr}_2\text{O}_7^{2-}$  in Water. *ACS Appl. Mater. Interfaces* **2018**, *10*, 16650–16659. [[CrossRef](#)]
63. Zhu, S.-Y.; Yan, B. A novel covalent post-synthetically modified MOF hybrid as a sensitive and selective fluorescent probe for  $\text{Al}^{3+}$  detection in aqueous media. *Dalton Trans.* **2018**, *47*, 1674–1681. [[CrossRef](#)]
64. Fajal, S.; Samanta, P.; Dutta, S.; Ghosh, S.K. Selective and sensitive recognition of  $\text{Fe}^{3+}$  ion by a Lewis basic functionalized chemically stable metal-organic framework (MOF). *Inorg. Chim. Acta* **2020**, *502*, 119359. [[CrossRef](#)]
65. Hibbard, H.A.J.; Burnley, M.J.; Rubin, H.N.; Miera, J.A.; Reynolds, M.M. Porphyrin-based metal-organic framework and polyvinylchloride composites for fluorescence sensing of divalent cadmium ions in water. *Inorg. Chem. Commun.* **2020**, *115*, 107861. [[CrossRef](#)]
66. Gogoi, C.; Nagarjun, N.; Roy, S.; Mostakim, S.K.; Volkmer, D.; Dhakshinamoorthy, A.; Biswas, S. A Zr-Based Metal–Organic Framework with a DUT-52 Structure Containing a Trifluoroacetamido-Functionalized Linker for Aqueous Phase Fluorescence Sensing of the Cyanide Ion and Aerobic Oxidation of Cyclohexane. *Inorg. Chem.* **2021**, *60*, 4539–4550. [[CrossRef](#)]
67. Li, J.; Yuan, S.; Qin, J.-S.; Pang, J.; Zhang, P.; Zhang, Y.; Huang, Y.; Drake, H.F.; Liu, W.R.; Zhou, H.-C. Stepwise Assembly of Turn-on Fluorescence Sensors in Multicomponent Metal–Organic Frameworks for in Vitro Cyanide Detection. *Angew. Chem. Int. Ed.* **2020**, *59*, 9319–9323. [[CrossRef](#)] [[PubMed](#)]
68. Kalaj, M.; Cohen, S.M. Postsynthetic Modification: An Enabling Technology for the Advancement of Metal–Organic Frameworks. *ACS Cent. Sci.* **2020**, *6*, 1046–1057. [[CrossRef](#)] [[PubMed](#)]
69. Zhu, S.-Y.; Yan, B. A novel sensitive fluorescent probe of  $\text{S}_2\text{O}_8^{2-}$  and  $\text{Fe}^{3+}$  based on covalent post-functionalization of a zirconium(IV) metal–organic framework. *Dalton Trans.* **2018**, *47*, 11586–11592. [[CrossRef](#)]
70. Zhu, S.; Zhao, L.; Yan, B. A novel spectroscopic probe for detecting food preservative  $\text{NO}_2^-$ : Citric acid functionalized metal-organic framework and luminescence sensing. *Microchem. J.* **2020**, *155*, 104768. [[CrossRef](#)]
71. Zhang, X.; Xia, T.; Jiang, K.; Cui, Y.; Yang, Y.; Qian, G. Highly sensitive and selective detection of mercury (II) based on a zirconium metal-organic framework in aqueous media. *J. Solid State Chem.* **2017**, *253*, 277–281. [[CrossRef](#)]
72. Zhang, Z.; Wei, Z.; Meng, F.; Su, J.; Chen, D.; Guo, Z.; Xing, H. RhB-Embedded Zirconium–Naphthalene-Based Metal–Organic Framework Composite as a Luminescent Self-Calibrating Platform for the Selective Detection of Inorganic Ions. *Chem. Eur. J.* **2020**, *26*, 1661–1667. [[CrossRef](#)]
73. Yang, L.; Liu, Y.; Chen, L.; Guo, L.; Lei, Y.; Wang, L. Stable dual-emissive fluorescein@UiO-67 metal-organic frameworks for visual and ratiometric sensing of  $\text{Al}^{3+}$  and ascorbic acid. *Spectrochim. Acta Part A Mol. Biomol. Spectrosc.* **2021**, *261*, 120068. [[CrossRef](#)] [[PubMed](#)]
74. Li, Y.; Wei, Z.; Zhang, Y.; Guo, Z.; Chen, D.; Jia, P.; Chen, P.; Xing, H. Dual-Emitting EY@Zr-MOF Composite as Self-Calibrating Luminescent Sensor for Selective Detection of Inorganic Ions and Nitroaromatics. *ACS Sustain. Chem. Eng.* **2019**, *7*, 6196–6203. [[CrossRef](#)]
75. Zheng, X.; Zhao, Y.; Jia, P.; Wang, Q.; Liu, Y.; Bu, T.; Zhang, M.; Bai, F.; Wang, L. Dual-Emission Zr-MOF-Based Composite Material as a Fluorescence Turn-On Sensor for the Ultrasensitive Detection of  $\text{Al}^{3+}$ . *Inorg. Chem.* **2020**, *59*, 18205–18213. [[CrossRef](#)] [[PubMed](#)]
76. Yang, L.; Liu, Y.-L.; Liu, C.-G.; Fu, Y.; Ye, F. A built-in self-calibrating luminescence sensor based on RhB@Zr-MOF for detection of cations, nitro explosives and pesticides. *RSC Adv.* **2020**, *10*, 19149–19156. [[CrossRef](#)]
77. Sk, M.; Biswas, S. A thiadiazole-functionalized Zr(IV)-based metal–organic framework as a highly fluorescent probe for the selective detection of picric acid. *CrystEngComm* **2016**, *18*, 3104–3113. [[CrossRef](#)]
78. Li, Q.-Y.; Ma, Z.; Zhang, W.-Q.; Xu, J.-L.; Wei, W.; Lu, H.; Zhao, X.; Wang, X.-J. AIE-active tetraphenylethene functionalized metal–organic framework for selective detection of nitroaromatic explosives and organic photocatalysis. *Chem. Commun.* **2016**, *52*, 11284–11287. [[CrossRef](#)]
79. Wang, B.; Lv, X.-L.; Feng, D.; Xie, L.-H.; Zhang, J.; Li, M.; Xie, Y.; Li, J.-R.; Zhou, H.-C. Highly Stable Zr(IV)-Based Metal–Organic Frameworks for the Detection and Removal of Antibiotics and Organic Explosives in Water. *J. Am. Chem. Soc.* **2016**, *138*, 6204–6216. [[CrossRef](#)]
80. Yang, J.-M.; Hu, X.-W.; Liu, Y.-X.; Zhang, W. Fabrication of a carbon quantum dots-immobilized zirconium-based metal-organic framework composite fluorescence sensor for highly sensitive detection of 4-nitrophenol. *Microporous Mesoporous Mater.* **2019**, *274*, 149–154. [[CrossRef](#)]
81. Sen Bishwas, M.; Malik, M.; Poddar, P. Raman spectroscopy-based sensitive, fast and reversible vapour phase detection of explosives adsorbed on metal–organic frameworks UiO-67. *N. J. Chem.* **2021**, *45*, 7145–7153. [[CrossRef](#)]
82. Ning, D.; Liu, Q.; Wang, Q.; Du, X.-M.; Li, Y.; Ruan, W.-J. Pyrene-based MOFs as fluorescent sensors for PAHs: An energetic pathway of the backbone structure effect on response. *Dalton Trans.* **2019**, *48*, 5705–5712. [[CrossRef](#)] [[PubMed](#)]
83. Drache, F.; Bon, V.; Senkovska, I.; Adam, M.; Eychmüller, A.; Kaskel, S. Vapochromic Luminescence of a Zirconium-Based Metal–Organic Framework for Sensing Applications. *Eur. J. Inorg. Chem.* **2016**, *2016*, 4483–4489. [[CrossRef](#)]

84. Zhang, W.-Q.; Li, Q.-Y.; Cheng, J.-Y.; Cheng, K.; Yang, X.; Li, Y.; Zhao, X.; Wang, X.-J. Ratiometric Luminescent Detection of Organic Amines Due to the Induced Lactam–Lactim Tautomerization of Organic Linker in a Metal–Organic Framework. *ACS Appl. Mater. Interfaces* **2017**, *9*, 31352–31356. [[CrossRef](#)] [[PubMed](#)]
85. Li, C.; Huang, J.; Zhu, H.; Liu, L.; Feng, Y.; Hu, G.; Yu, X. Dual-emitting fluorescence of Eu/Zr-MOF for ratiometric sensing formaldehyde. *Sens. Actuators B Chem.* **2017**, *253*, 275–282. [[CrossRef](#)]
86. Rouschmeyer, P.; Guillou, N.; Serre, C.; Clavier, G.; Martineau, C.; Audebert, P.; Elkaïm, E.; Allain, C.; Devic, T. A Flexible Fluorescent Zr Carboxylate Metal–Organic Framework for the Detection of Electron-Rich Molecules in Solution. *Inorg. Chem.* **2017**, *56*, 8423–8429. [[CrossRef](#)]
87. Wei, Z.; Chen, D.; Guo, Z.; Jia, P.; Xing, H. Eosin Y-Embedded Zirconium-Based Metal–Organic Framework as a Dual-Emitting Built-In Self-Calibrating Platform for Pesticide Detection. *Inorg. Chem.* **2020**, *59*, 5386–5393. [[CrossRef](#)]
88. Li, W.-J.; Chang, L.; Liu, Q.; Ning, D.; Yao, X.-Y.; Li, Y.; Ruan, W.-J. Enzyme-Assisted Metal–Organic Framework Sensing System for Diethylstilbestrol Detection. *Chem. Eur. J.* **2017**, *23*, 15498–15504. [[CrossRef](#)]
89. Yang, H.; Wang, B.; Cheng, J.; Wang, R.; Zhang, S.; Dong, S.; Wei, S.; Wang, P.; Li, J.-R. Determination and removal of clenbuterol with a stable fluorescent zirconium(IV)-based metal organic framework. *Microchim. Acta* **2019**, *186*, 454. [[CrossRef](#)]
90. Liu, S.; Bai, J.; Huo, Y.; Ning, B.; Peng, Y.; Li, S.; Han, D.; Kang, W.; Gao, Z. A zirconium-porphyrin MOF-based ratiometric biosensor for rapid and ultrasensitive detection of chloramphenicol. *Biosens. Bioelectron.* **2020**, *149*, 111801. [[CrossRef](#)]
91. Xu, X.-Y.; Yan, B. Selective detection and controlled release of Aspirin over fluorescent amino-functionalized metal–organic framework in aqueous solution. *Sens. Actuators B Chem.* **2016**, *230*, 463–469. [[CrossRef](#)]
92. Yang, Q.; Hong, H.; Luo, Y. Heterogeneous nucleation and synthesis of carbon dots hybrid Zr-based MOFs for simultaneous recognition and effective removal of tetracycline. *Chem. Eng. J.* **2020**, *392*, 123680. [[CrossRef](#)]
93. Zhou, Y.; Yang, Q.; Zhang, D.; Gan, N.; Li, Q.; Cuan, J. Detection and removal of antibiotic tetracycline in water with a highly stable luminescent MOF. *Sens. Actuators B Chem.* **2018**, *262*, 137–143. [[CrossRef](#)]
94. Zhang, H.-T.; Zhang, J.-W.; Huang, G.; Du, Z.-Y.; Jiang, H.-L. An amine-functionalized metal–organic framework as a sensing platform for DNA detection. *Chem. Commun.* **2014**, *50*, 12069–12072. [[CrossRef](#)] [[PubMed](#)]
95. Desai, A.V.; Samanta, P.; Manna, B.; Ghosh, S.K. Aqueous phase nitric oxide detection by an amine-decorated metal–organic framework. *Chem. Commun.* **2015**, *51*, 6111–6114. [[CrossRef](#)]
96. Wang, N.; Xie, M.; Wang, M.; Li, Z.; Su, X. UiO-66-NH<sub>2</sub> MOF-based ratiometric fluorescent probe for the detection of dopamine and reduced glutathione. *Talanta* **2020**, *220*, 121352. [[CrossRef](#)]
97. Li, Y.-A.; Zhao, C.-W.; Zhu, N.-X.; Liu, Q.-K.; Chen, G.-J.; Liu, J.-B.; Zhao, X.-D.; Ma, J.-P.; Zhang, S.; Dong, Y.-B. Nanoscale UiO-MOF-based luminescent sensors for highly selective detection of cysteine and glutathione and their application in bioimaging. *Chem. Commun.* **2015**, *51*, 17672–17675. [[CrossRef](#)]
98. Gui, B.; Meng, Y.; Xie, Y.; Tian, J.; Yu, G.; Zeng, W.; Zhang, G.; Gong, S.; Yang, C.; Zhang, D.; et al. Tuning the Photoinduced Electron Transfer in a Zr-MOF: Toward Solid-State Fluorescent Molecular Switch and Turn-On Sensor. *Adv. Mater.* **2018**, *30*, 1802329. [[CrossRef](#)] [[PubMed](#)]
99. Gong, M.; Yang, J.; Li, Y.; Zhuang, Q.; Gu, J. Substitution-type luminescent MOF sensor with built-in capturer for selective cholesterol detection in blood serum. *J. Mater. Chem. C* **2019**, *7*, 12674–12681. [[CrossRef](#)]
100. Xia, C.; Xu, Y.; Cao, M.-M.; Liu, Y.-P.; Xia, J.-F.; Jiang, D.-Y.; Zhou, G.-H.; Xie, R.-J.; Zhang, D.-F.; Li, H.-L. A selective and sensitive fluorescent probe for bilirubin in human serum based on europium(III) post-functionalized Zr(IV)-Based MOFs. *Talanta* **2020**, *212*, 120795. [[CrossRef](#)]
101. Zhang, X.; Zhang, W.; Li, G.; Liu, Q.; Xu, Y.; Liu, X. A ratiometric fluorescent probe for determination of the anthrax biomarker 2,6-pyridinedicarboxylic acid based on a terbium(III)-functionalized UiO-67 metal-organic framework. *Microchim. Acta* **2020**, *187*, 122. [[CrossRef](#)]
102. Sun, Z.; Wu, S.; Ma, J.; Shi, H.; Wang, L.; Sheng, A.; Yin, T.; Sun, L.; Li, G. Colorimetric Sensor Array for Human Semen Identification Designed by Coupling Zirconium Metal–Organic Frameworks with DNA-Modified Gold Nanoparticles. *ACS Appl. Mater. Interfaces* **2019**, *11*, 36316–36323. [[CrossRef](#)]
103. Nickerl, G.; Senkovska, I.; Kaskel, S. Tetrazine functionalized zirconium MOF as an optical sensor for oxidizing gases. *Chem. Commun.* **2015**, *51*, 2280–2282. [[CrossRef](#)]
104. Nandi, S.; Banesh, S.; Trivedi, V.; Biswas, S. A dinitro-functionalized metal–organic framework featuring visual and fluorogenic sensing of H<sub>2</sub>S in living cells, human blood plasma and environmental samples. *Analyst* **2018**, *143*, 1482–1491. [[CrossRef](#)] [[PubMed](#)]
105. Gogoi, C.; Kumar, A.; Sk, M.; Biswas, S. Specific fluorescence sensing of hydrogen sulphide by an azide functionalized Zr(IV) MOF with DUT-52 topology. *Microporous Mesoporous Mater.* **2021**, *311*, 110725. [[CrossRef](#)]
106. Guo, L.; Wang, M.; Cao, D. A Novel Zr-MOF as Fluorescence Turn-On Probe for Real-Time Detecting H<sub>2</sub>S Gas and Fingerprint Identification. *Small* **2018**, *14*, 1703822. [[CrossRef](#)] [[PubMed](#)]
107. Yang, Y.; Liu, X.; Yan, D.; Deng, P.; Guo, Z.; Zhan, H. Europium ion post-functionalized zirconium metal–organic frameworks as luminescent probes for effectively sensing hydrazine hydrate. *RSC Adv.* **2018**, *8*, 17471–17476. [[CrossRef](#)]
108. Sk, M.; Khan, M.R.U.Z.; Das, A.; Nandi, S.; Trivedi, V.; Biswas, S. A phthalimide-functionalized UiO-66 metal–organic framework for the fluorogenic detection of hydrazine in live cells. *Dalton Trans.* **2019**, *48*, 12615–12621. [[CrossRef](#)] [[PubMed](#)]

109. Sk, M.; Banesh, S.; Trivedi, V.; Biswas, S. Selective and Sensitive Sensing of Hydrogen Peroxide by a Boronic Acid Functionalized Metal–Organic Framework and Its Application in Live-Cell Imaging. *Inorg. Chem.* **2018**, *57*, 14574–14581. [[CrossRef](#)]
110. Ghosh, S.; Das, A.; Biswas, S. A functionalized UiO-66 MOF acting as a luminescent chemosensor for selective and sensitive turn-on detection of superoxide and acetylacetone. *Microporous Mesoporous Mater.* **2021**, *323*, 111251. [[CrossRef](#)]
111. Das, A.; Anbu, N.; Sk, M.; Dhakshinamoorthy, A.; Biswas, S. A functionalized UiO-66 MOF for turn-on fluorescence sensing of superoxide in water and efficient catalysis for Knoevenagel condensation. *Dalton Trans.* **2019**, *48*, 17371–17380. [[CrossRef](#)]
112. Li, Q.-Y.; Li, Y.-A.; Guan, Q.; Li, W.-Y.; Dong, X.-J.; Dong, Y.-B. UiO-68-PT MOF-Based Sensor and Its Mixed Matrix Membrane for Detection of HClO in Water. *Inorg. Chem.* **2019**, *58*, 9890–9896. [[CrossRef](#)] [[PubMed](#)]
113. Jiang, H.-L.; Feng, D.; Wang, K.; Gu, Z.-Y.; Wei, Z.; Chen, Y.-P.; Zhou, H.-C. An Exceptionally Stable, Porphyrinic Zr Metal–Organic Framework Exhibiting pH-Dependent Fluorescence. *J. Am. Chem. Soc.* **2013**, *135*, 13934–13938. [[CrossRef](#)]
114. Chen, H.; Wang, J.; Shan, D.; Chen, J.; Zhang, S.; Lu, X. Dual-Emitting Fluorescent Metal–Organic Framework Nanocomposites as a Broad-Range pH Sensor for Fluorescence Imaging. *Anal. Chem.* **2018**, *90*, 7056–7063. [[CrossRef](#)] [[PubMed](#)]
115. Deibert, B.J.; Li, J. A distinct reversible colorimetric and fluorescent low pH response on a water-stable zirconium–porphyrin metal–organic framework. *Chem. Commun.* **2014**, *50*, 9636–9639. [[CrossRef](#)]
116. Sousaraei, A.; Queirós, C.; Moscoso, F.G.; Silva, A.M.G.; Lopes-Costa, T.; Pedrosa, J.M.; Cunha-Silva, L.; Cabanillas-Gonzalez, J. Reversible Protonation of Porphyrinic Metal–Organic Frameworks Embedded in Nanoporous Polydimethylsiloxane for Colorimetric Sensing. *Adv. Mater. Interfaces* **2021**, *8*, 2001759. [[CrossRef](#)]
117. Moon, S.-Y.; Howarth, A.J.; Wang, T.; Vermeulen, N.A.; Hupp, J.T.; Farha, O.K. A visually detectable pH responsive zirconium metal–organic framework. *Chem. Commun.* **2016**, *52*, 3438–3441. [[CrossRef](#)]
118. Aguilera-Sigalat, J.; Bradshaw, D. A colloidal water-stable MOF as a broad-range fluorescent pH sensor via post-synthetic modification. *Chem. Commun.* **2014**, *50*, 4711–4713. [[CrossRef](#)]
119. Sk, M.; Nandi, S.; Singh, R.K.; Trivedi, V.; Biswas, S. Selective Sensing of Peroxynitrite by Hf-Based UiO-66-B(OH)<sub>2</sub> Metal–Organic Framework: Applicability to Cell Imaging. *Inorg. Chem.* **2018**, *57*, 10128–10136. [[CrossRef](#)]
120. Dalapati, R.; Nandi, S.; Biswas, S. Post-synthetic modification of a metal–organic framework with a chemodosimeter for the rapid detection of lethal cyanide via dual emission. *Dalton Trans.* **2020**, *49*, 8684–8692. [[CrossRef](#)] [[PubMed](#)]
121. Nandi, S.; Biswas, S. A diamino functionalized metal-organic framework for fluorometric recognition of free chlorine in environmental water samples. *Microporous Mesoporous Mater.* **2020**, *299*, 110116. [[CrossRef](#)]
122. Wu, K.; Zheng, J.; Huang, Y.-L.; Luo, D.; Li, Y.Y.; Lu, W.; Li, D. Cr<sub>2</sub>O<sub>7</sub><sup>2-</sup> inside Zr/Hf-based metal–organic frameworks: Highly sensitive and selective detection and crystallographic evidence. *J. Mater. Chem. C* **2020**, *8*, 16974–16983. [[CrossRef](#)]
123. Xing, K.; Fan, R.-Q.; Liu, X.-Y.; Gai, S.; Chen, W.; Yang, Y.-L.; Li, J. A self-calibrating dual responsive platform for the sensitive detection of sulfite and sulfonic derivatives based on a robust Hf(IV) metal–organic framework. *Chem. Commun.* **2020**, *56*, 631–634. [[CrossRef](#)]
124. Xu, H.; Gao, J.; Qian, X.; Wang, J.; He, H.; Cui, Y.; Yang, Y.; Wang, Z.; Qian, G. Metal–organic framework nanosheets for fast-response and highly sensitive luminescent sensing of Fe<sup>3+</sup>. *J. Mater. Chem. A* **2016**, *4*, 10900–10905. [[CrossRef](#)]
125. Zhong, F.; Li, C.; Xie, Y.; Xu, H.; Gao, J. Titanium metal-organic framework nanorods for highly sensitive nitroaromatic explosives detection and nanomolar sensing of Fe<sup>3+</sup>. *J. Solid State Chem.* **2019**, *278*, 120892. [[CrossRef](#)]
126. Kaur, M.; Mehta, S.K.; Kansal, S.K. Amine-functionalized titanium metal-organic framework (NH<sub>2</sub>-MIL-125(Ti)): A novel fluorescent sensor for the highly selective sensing of copper ions. *Mater. Chem. Phys.* **2020**, *254*, 123539. [[CrossRef](#)]
127. Zhang, X.; Yan, Y.; Chen, F.; Bai, G.; Xu, H.; Xu, S. A Fluorescent Titanium-based Metal-Organic Framework Sensor for Nitroaromatics Detection. *Z. Anorg. Allg. Chem.* **2021**, *647*, 759–763. [[CrossRef](#)]
128. Jia, C.; Bai, J.; Liu, Z.; Gao, S.; Han, Y.; Yan, H. Application of a titanium-based metal-organic framework to protein kinase activity detection and inhibitor screening. *Anal. Chim. Acta* **2020**, *1128*, 99–106. [[CrossRef](#)]
129. Rogge, S.M.J.; Yot, P.G.; Jacobsen, J.; Muniz-Miranda, F.; Vandenbrande, S.; Gosch, J.; Ortiz, V.; Collings, I.E.; Devautour-Vinot, S.; Maurin, G.; et al. Charting the Metal-Dependent High-Pressure Stability of Bimetallic UiO-66 Materials. *ACS Mater. Lett.* **2020**, *2*, 438–445. [[CrossRef](#)]
130. Islamoglu, T.; Atilgan, A.; Moon, S.-Y.; Peterson, G.W.; DeCoste, J.B.; Hall, M.; Hupp, J.T.; Farha, O.K. Cerium(IV) vs Zirconium(IV) Based Metal–Organic Frameworks for Detoxification of a Nerve Agent. *Chem. Mater.* **2017**, *29*, 2672–2675. [[CrossRef](#)]
131. He, X.; Looker, B.G.; Dinh, K.T.; Stubbs, A.W.; Chen, T.; Meyer, R.J.; Serna, P.; Román-Leshkov, Y.; Lancaster, K.M.; Dincă, M. Cerium(IV) Enhances the Catalytic Oxidation Activity of Single-Site Cu Active Sites in MOFs. *ACS Catal.* **2020**, *10*, 7820–7825. [[CrossRef](#)]
132. Yue, D.; Zhao, D.; Zhang, J.; Zhang, L.; Jiang, K.; Zhang, X.; Cui, Y.; Yang, Y.; Chen, B.; Qian, G. A luminescent cerium metal–organic framework for the turn-on sensing of ascorbic acid. *Chem. Commun.* **2017**, *53*, 11221–11224. [[CrossRef](#)]
133. Yang, Y.; Zhu, W.; Sun, B.; Hu, H.; Li, X.; Bao, S.; Su, Z. Two fluorescent cerium metal-organic frameworks for the “turn-on” sensing of AA with high sensitivity as well as biological and electrochemical properties. *J. Solid State Chem.* **2021**, *302*, 122376. [[CrossRef](#)]
134. Dalapati, R.; Sakthivel, B.; Ghosal, M.K.; Dhakshinamoorthy, A.; Biswas, S. A cerium-based metal–organic framework having inherent oxidase-like activity applicable for colorimetric sensing of biothiols and aerobic oxidation of thiols. *CrystEngComm* **2017**, *19*, 5915–5925. [[CrossRef](#)]

135. Wang, C.; Tang, G.; Tan, H. Colorimetric determination of mercury(II) via the inhibition by ssDNA of the oxidase-like activity of a mixed valence state cerium-based metal-organic framework. *Microchim. Acta* **2018**, *185*, 475. [[CrossRef](#)] [[PubMed](#)]
136. Chen, A.; Chatterjee, S. Nanomaterials based electrochemical sensors for biomedical applications. *Chem. Soc. Rev.* **2013**, *42*, 5425–5438. [[CrossRef](#)]
137. Wang, J. Electrochemical Glucose Biosensors. *Chem. Rev.* **2008**, *108*, 814–825. [[CrossRef](#)] [[PubMed](#)]
138. Wang, J. Glucose Biosensors: 40 Years of Advances and Challenges. *Electroanalysis* **2001**, *13*, 983–988. [[CrossRef](#)]
139. Murray, R.W. Chemically modified electrodes. *Acc. Chem. Res.* **1980**, *13*, 135–141. [[CrossRef](#)]
140. Liu, L.; Zhou, Y.; Liu, S.; Xu, M. The Applications of Metal–Organic Frameworks in Electrochemical Sensors. *ChemElectroChem* **2018**, *5*, 6–19. [[CrossRef](#)]
141. Kempahanumakkagari, S.; Vellingiri, K.; Deep, A.; Kwon, E.E.; Bolan, N.; Kim, K.-H. Metal–organic framework composites as electrocatalysts for electrochemical sensing applications. *Coord. Chem. Rev.* **2018**, *357*, 105–129. [[CrossRef](#)]
142. Chuang, C.-H.; Kung, C.-W. Metal–Organic Frameworks toward Electrochemical Sensors: Challenges and Opportunities. *Electroanalysis* **2020**, *32*, 1885–1895. [[CrossRef](#)]
143. Kung, C.-W.; Goswami, S.; Hod, I.; Wang, T.C.; Duan, J.; Farha, O.K.; Hupp, J.T. Charge Transport in Zirconium-Based Metal–Organic Frameworks. *Acc. Chem. Res.* **2020**, *53*, 1187–1195. [[CrossRef](#)]
144. Xie, L.S.; Skorupskii, G.; Dincă, M. Electrically Conductive Metal–Organic Frameworks. *Chem. Rev.* **2020**, *120*, 8536–8580. [[CrossRef](#)] [[PubMed](#)]
145. Ling, S.; Slater, B. Unusually Large Band Gap Changes in Breathing Metal–Organic Framework Materials. *J. Phys. Chem. C* **2015**, *119*, 16667–16677. [[CrossRef](#)]
146. Hendrickx, K.; Vanpoucke, D.E.P.; Leus, K.; Lejaeghere, K.; Van Yperen-De Deyne, A.; Van Speybroeck, V.; Van Der Voort, P.; Hemelsoet, K. Understanding Intrinsic Light Absorption Properties of UiO-66 Frameworks: A Combined Theoretical and Experimental Study. *Inorg. Chem.* **2015**, *54*, 10701–10710. [[CrossRef](#)] [[PubMed](#)]
147. Kung, C.-W.; Han, P.-C.; Chuang, C.-H.; Wu, K.C.-W. Electronically conductive metal–organic framework-based materials. *APL Mater.* **2019**, *7*, 110902. [[CrossRef](#)]
148. Wang, T.C.; Hod, I.; Audu, C.O.; Vermeulen, N.A.; Nguyen, S.T.; Farha, O.K.; Hupp, J.T. Rendering High Surface Area, Mesoporous Metal–Organic Frameworks Electronically Conductive. *ACS Appl. Mater. Interfaces* **2017**, *9*, 12584–12591. [[CrossRef](#)]
149. Goswami, S.; Ray, D.; Otake, K.-i.; Kung, C.-W.; Garibay, S.J.; Islamoglu, T.; Atilgan, A.; Cui, Y.; Cramer, C.J.; Farha, O.K.; et al. A porous, electrically conductive hexa-zirconium(IV) metal-organic framework. *Chem. Sci.* **2018**, *9*, 4477–4482. [[CrossRef](#)]
150. Kung, C.-W.; Otake, K.; Buru, C.T.; Goswami, S.; Cui, Y.; Hupp, J.T.; Spokoiny, A.M.; Farha, O.K. Increased Electrical Conductivity in a Mesoporous Metal–Organic Framework Featuring Metallacarboranes Guests. *J. Am. Chem. Soc.* **2018**, *140*, 3871–3875. [[CrossRef](#)]
151. Chen, Y.-C.; Chiang, W.-H.; Kurniawan, D.; Yeh, P.-C.; Otake, K.-i.; Kung, C.-W. Impregnation of Graphene Quantum Dots into a Metal–Organic Framework to Render Increased Electrical Conductivity and Activity for Electrochemical Sensing. *ACS Appl. Mater. Interfaces* **2019**, *11*, 35319–35326. [[CrossRef](#)]
152. Ray, D.; Goswami, S.; Duan, J.; Hupp, J.T.; Cramer, C.J.; Gagliardi, L. Tuning the Conductivity of Hexa-Zirconium(IV) Metal–Organic Frameworks by Encapsulating Heterofullerenes. *Chem. Mater.* **2021**, *33*, 1182–1189. [[CrossRef](#)]
153. Blauch, D.N.; Saveant, J.M. Dynamics of electron hopping in assemblies of redox centers. Percolation and diffusion. *J. Am. Chem. Soc.* **1992**, *114*, 3323–3332. [[CrossRef](#)]
154. Kung, C.-W.; Wang, T.C.; Mondloch, J.E.; Fairen-Jimenez, D.; Gardner, D.M.; Bury, W.; Klingsporn, J.M.; Barnes, J.C.; Van Deyne, R.; Stoddart, J.F.; et al. Metal–Organic Framework Thin Films Composed of Free-Standing Acicular Nanorods Exhibiting Reversible Electrochromism. *Chem. Mater.* **2013**, *25*, 5012–5017. [[CrossRef](#)]
155. Lin, S.; Usov, P.M.; Morris, A.J. The role of redox hopping in metal–organic framework electrocatalysis. *Chem. Commun.* **2018**, *54*, 6965–6974. [[CrossRef](#)]
156. Usov, P.M.; Fabian, C.; D’Alessandro, D.M. Rapid determination of the optical and redox properties of a metal–organic framework via in situ solid state spectroelectrochemistry. *Chem. Commun.* **2012**, *48*, 3945–3947. [[CrossRef](#)]
157. Ahrenholtz, S.R.; Epley, C.C.; Morris, A.J. Solvothermal Preparation of an Electrocatalytic Metalloporphyrin MOF Thin Film and its Redox Hopping Charge-Transfer Mechanism. *J. Am. Chem. Soc.* **2014**, *136*, 2464–2472. [[CrossRef](#)] [[PubMed](#)]
158. Hod, I.; Sampson, M.D.; Deria, P.; Kubiak, C.P.; Farha, O.K.; Hupp, J.T. Fe-Porphyrin-Based Metal–Organic Framework Films as High-Surface Concentration, Heterogeneous Catalysts for Electrochemical Reduction of CO<sub>2</sub>. *ACS Catal.* **2015**, *5*, 6302–6309. [[CrossRef](#)]
159. Fei, H.; Pullen, S.; Wagner, A.; Ott, S.; Cohen, S.M. Functionalization of robust Zr(IV)-based metal-organic framework films via a postsynthetic ligand exchange. *Chem. Commun.* **2015**, *51*, 66–69. [[CrossRef](#)]
160. Johnson, B.A.; Bhunia, A.; Fei, H.; Cohen, S.M.; Ott, S. Development of a UiO-Type Thin Film Electrocatalysis Platform with Redox-Active Linkers. *J. Am. Chem. Soc.* **2018**, *140*, 2985–2994. [[CrossRef](#)] [[PubMed](#)]
161. Shimoni, R.; He, W.; Liberman, I.; Hod, I. Tuning of Redox Conductivity and Electrocatalytic Activity in Metal–Organic Framework Films Via Control of Defect Site Density. *J. Phys. Chem. C* **2019**, *123*, 5531–5539. [[CrossRef](#)]
162. Maindan, K.; Li, X.; Yu, J.; Deria, P. Controlling Charge-Transport in Metal–Organic Frameworks: Contribution of Topological and Spin-State Variation on the Iron–Porphyrin Centered Redox Hopping Rate. *J. Phys. Chem. B* **2019**, *123*, 8814–8822. [[CrossRef](#)] [[PubMed](#)]

163. Chuang, C.-H.; Li, J.-H.; Chen, Y.-C.; Wang, Y.-S.; Kung, C.-W. Redox-Hopping and Electrochemical Behaviors of Metal–Organic Framework Thin Films Fabricated by Various Approaches. *J. Phys. Chem. C* **2020**, *124*, 20854–20863. [CrossRef]
164. Shen, C.-H.; Chuang, C.-H.; Gu, Y.-J.; Ho, W.H.; Song, Y.-D.; Chen, Y.-C.; Wang, Y.-C.; Kung, C.-W. Cerium-Based Metal–Organic Framework Nanocrystals Interconnected by Carbon Nanotubes for Boosting Electrochemical Capacitor Performance. *ACS Appl. Mater. Interfaces* **2021**, *13*, 16418–16426. [CrossRef] [PubMed]
165. Amombo Noa, F.M.; Abrahamsson, M.; Ahlberg, E.; Cheung, O.; Göb, C.R.; McKenzie, C.J.; Öhrström, L. A unified topology approach to dot-, rod-, and sheet-MOFs. *Chem* **2021**, *7*, 2491–2512. [CrossRef]
166. Kung, C.-W.; Chang, T.-H.; Chou, L.-Y.; Hupp, J.T.; Farha, O.K.; Ho, K.-C. Porphyrin-based metal–organic framework thin films for electrochemical nitrite detection. *Electrochem. Commun.* **2015**, *58*, 51–56. [CrossRef]
167. Kung, C.-W.; Li, Y.-S.; Lee, M.-H.; Wang, S.-Y.; Chiang, W.-H.; Ho, K.-C. In situ growth of porphyrinic metal–organic framework nanocrystals on graphene nanoribbons for the electrocatalytic oxidation of nitrite. *J. Mater. Chem. A* **2016**, *4*, 10673–10682. [CrossRef]
168. Su, C.-H.; Kung, C.-W.; Chang, T.-H.; Lu, H.-C.; Ho, K.-C.; Liao, Y.-C. Inkjet-printed porphyrinic metal–organic framework thin films for electrocatalysis. *J. Mater. Chem. A* **2016**, *4*, 11094–11102. [CrossRef]
169. Wang, Y.-C.; Chen, Y.-C.; Chuang, W.-S.; Li, J.-H.; Wang, Y.-S.; Chuang, C.-H.; Chen, C.-Y.; Kung, C.-W. Pore-Confined Silver Nanoparticles in a Porphyrinic Metal–Organic Framework for Electrochemical Nitrite Detection. *ACS Appl. Nano Mater.* **2020**, *3*, 9440–9448. [CrossRef]
170. Pila, T.; Chirawatikul, P.; Piyakeeratikul, P.; Somjit, V.; Sawangphruk, M.; Kongpatpanich, K. Metalloporphyrin-Based Metal–Organic Frameworks on Flexible Carbon Paper for Electrocatalytic Nitrite Oxidation. *Chem. Eur. J.* **2020**, *26*, 17399–17404. [CrossRef]
171. Ling, P.; Lei, J.; Ju, H. Porphyrinic metal–organic framework as electrochemical probe for DNA sensing via triple-helix molecular switch. *Biosens. Bioelectron.* **2015**, *71*, 373–379. [CrossRef] [PubMed]
172. Zhang, G.-Y.; Zhuang, Y.-H.; Shan, D.; Su, G.-F.; Cosnier, S.; Zhang, X.-J. Zirconium-Based Porphyrinic Metal–Organic Framework (PCN-222): Enhanced Photoelectrochemical Response and Its Application for Label-Free Phosphoprotein Detection. *Anal. Chem.* **2016**, *88*, 11207–11212. [CrossRef] [PubMed]
173. Wang, Y.; Wang, L.; Chen, H.; Hu, X.; Ma, S. Fabrication of Highly Sensitive and Stable Hydroxylamine Electrochemical Sensor Based on Gold Nanoparticles and Metal–Metalloporphyrin Framework Modified Electrode. *ACS Appl. Mater. Interfaces* **2016**, *8*, 18173–18181. [CrossRef]
174. Huang, T.Y.; Kung, C.W.; Liao, Y.T.; Kao, S.Y.; Cheng, M.; Chang, T.H.; Henzie, J.; Alamri Hatem, R.; Allothman Zeid, A.; Yamauchi, Y.; et al. Enhanced Charge Collection in MOF-525–PEDOT Nanotube Composites Enable Highly Sensitive Biosensing. *Adv. Sci.* **2017**, *4*, 1700261. [CrossRef] [PubMed]
175. Cao, M.; Yin, X.; Bo, X.; Guo, L. High-performance electrocatalyst based on metal–organic framework/macroporous carbon composite for efficient detection of luteolin. *J. Electroanal. Chem.* **2018**, *824*, 153–160. [CrossRef]
176. Yu, G.; Song, X.; Zheng, S.; Zhao, Q.; Yan, D.; Zhao, J. A facile and sensitive tetrabromobisphenol-A sensor based on biomimetic catalysis of a metal–organic framework: PCN-222(Fe). *Anal. Methods* **2018**, *10*, 4275–4281. [CrossRef]
177. Zhang, J.; Qiang, Y.; Xu, X. An Ultrasensitive Electrochemical Aptasensor for Thrombin Detection Using MoS<sub>2</sub> Nanoparticles Loaded Iron-Porphyrinic Metal–Organic Framework as Signal Amplifier. *J. Electrochem. Soc.* **2020**, *167*, 087503. [CrossRef]
178. Zhang, J.; Xu, X.; Qiang, Y. Ultrasensitive electrochemical aptasensor for ochratoxin A detection using AgPt bimetallic nanoparticles decorated iron-porphyrinic metal–organic framework for signal amplification. *Sens. Actuators B Chem.* **2020**, *312*, 127964. [CrossRef]
179. Wei, C.; Zhou, H.; Liu, Q. PCN-222 MOF decorated conductive PEDOT films for sensitive electrochemical determination of chloramphenicol. *Mater. Chem. Phys.* **2021**, *270*, 124831. [CrossRef]
180. Zhou, Z.; Mukherjee, S.; Hou, S.; Li, W.; Elsner, M.; Fischer, R.A. Porphyrinic MOF Film for Multifaceted Electrochemical Sensing. *Angew. Chem. Int. Ed.* **2021**, *60*, 20551–20557. [CrossRef]
181. Su, F.; Zhang, S.; Ji, H.; Zhao, H.; Tian, J.-Y.; Liu, C.-S.; Zhang, Z.; Fang, S.; Zhu, X.; Du, M. Two-Dimensional Zirconium-Based Metal–Organic Framework Nanosheet Composites Embedded with Au Nanoclusters: A Highly Sensitive Electrochemical Aptasensor toward Detecting Cocaine. *ACS Sens.* **2017**, *2*, 998–1005. [CrossRef]
182. Deng, M.; Lin, S.; Bo, X.; Guo, L. Simultaneous and sensitive electrochemical detection of dihydroxybenzene isomers with UiO-66 metal–organic framework/mesoporous carbon. *Talanta* **2017**, *174*, 527–538. [CrossRef]
183. Deng, M.; Bo, X.; Guo, L. Encapsulation of platinum nanoparticles into a series of zirconium-based metal–organic frameworks: Effect of the carrier structures on electrocatalytic performances of composites. *J. Electroanal. Chem.* **2018**, *815*, 198–209. [CrossRef]
184. Liu, H.; Hassan, M.; Bo, X.; Guo, L. Fumarate-based metal–organic framework/mesoporous carbon as a novel electrochemical sensor for the detection of gallic acid and luteolin. *J. Electroanal. Chem.* **2019**, *849*, 113378. [CrossRef]
185. Du, L.; Chen, W.; Wang, J.; Cai, W.; Kong, S.; Wu, C. Folic acid-functionalized zirconium metal–organic frameworks based electrochemical impedance biosensor for the cancer cell detection. *Sens. Actuators B Chem.* **2019**, *301*, 127073. [CrossRef]
186. Li, Y.; Hu, M.; Huang, X.; Wang, M.; He, L.; Song, Y.; Jia, Q.; Zhou, N.; Zhang, Z.; Du, M. Multicomponent zirconium-based metal–organic frameworks for impedimetric aptasensing of living cancer cells. *Sens. Actuators B Chem.* **2020**, *306*, 127608. [CrossRef]

187. Fang, X.; Chen, X.; Liu, Y.; Li, Q.; Zeng, Z.; Maiyalagan, T.; Mao, S. Nanocomposites of Zr(IV)-Based Metal–Organic Frameworks and Reduced Graphene Oxide for Electrochemically Sensing Ciprofloxacin in Water. *ACS Appl. Nano Mater.* **2019**, *2*, 2367–2376. [[CrossRef](#)]
188. Wang, H.; Bo, X.; Zhou, M.; Guo, L. DUT-67 and tubular polypyrrole formed a cross-linked network for electrochemical detection of nitrofurazone and ornidazole. *Anal. Chim. Acta* **2020**, *1109*, 1–8. [[CrossRef](#)]
189. Wang, Q.; Gu, C.; Fu, Y.; Liu, L.; Xie, Y. Ultrasensitive Electrochemical Sensor for Luteolin Based on Zirconium Metal–Organic Framework UiO-66/Reduced Graphene Oxide Composite Modified Glass Carbon Electrode. *Molecules* **2020**, *25*, 4557. [[CrossRef](#)] [[PubMed](#)]
190. Biswas, S.; Lan, Q.; Xie, Y.; Sun, X.; Wang, Y. Label-Free Electrochemical Immunosensor for Ultrasensitive Detection of Carbohydrate Antigen 125 Based on Antibody-Immobilized Biocompatible MOF-808/CNT. *ACS Appl. Mater. Interfaces* **2021**, *13*, 3295–3302. [[CrossRef](#)]
191. Ho, W.H.; Chen, T.-Y.; Otake, K.-i.; Chen, Y.-C.; Wang, Y.-S.; Li, J.-H.; Chen, H.-Y.; Kung, C.-W. Polyoxometalate adsorbed in a metal–organic framework for electrocatalytic dopamine oxidation. *Chem. Commun.* **2020**, *56*, 11763–11766. [[CrossRef](#)]
192. Chang, T.-E.; Chuang, C.-H.; Kung, C.-W. An iridium-decorated metal–organic framework for electrocatalytic oxidation of nitrite. *Electrochem. Commun.* **2021**, *122*, 106899. [[CrossRef](#)]
193. Yang, J.; Yang, L.; Ye, H.; Zhao, F.; Zeng, B. Highly dispersed AuPd alloy nanoparticles immobilized on UiO-66-NH<sub>2</sub> metal-organic framework for the detection of nitrite. *Electrochim. Acta* **2016**, *219*, 647–654. [[CrossRef](#)]
194. Wang, Y.; Wang, L.; Huang, W.; Zhang, T.; Hu, X.; Perman, J.A.; Ma, S. A metal–organic framework and conducting polymer based electrochemical sensor for high performance cadmium ion detection. *J. Mater. Chem. A* **2017**, *5*, 8385–8393. [[CrossRef](#)]
195. Chang, Y.-S.; Li, J.-H.; Chen, Y.-C.; Ho, W.H.; Song, Y.-D.; Kung, C.-W. Electrodeposition of pore-confined cobalt in metal–organic framework thin films toward electrochemical H<sub>2</sub>O<sub>2</sub> detection. *Electrochim. Acta* **2020**, *347*, 136276. [[CrossRef](#)]
196. Xu, Q.; Wang, Y.; Jin, G.; Jin, D.; Li, K.; Mao, A.; Hu, X. Photooxidation assisted sensitive detection of trace Mn<sup>2+</sup> in tea by NH<sub>2</sub>-MIL-125 (Ti) modified carbon paste electrode. *Sens. Actuators B Chem.* **2014**, *201*, 274–280. [[CrossRef](#)]
197. Jin, D.; Xu, Q.; Yu, L.; Hu, X. Photoelectrochemical detection of the herbicide clethodim by using the modified metal-organic framework amino-MIL-125(Ti)/TiO<sub>2</sub>. *Microchim. Acta* **2015**, *182*, 1885–1892. [[CrossRef](#)]
198. Dong, P.; Zhu, L.; Huang, J.; Ren, J.; Lei, J. Electrocatalysis of cerium metal-organic frameworks for ratiometric electrochemical detection of telomerase activity. *Biosens. Bioelectron.* **2019**, *138*, 111313. [[CrossRef](#)]
199. Wang, X.; Shi, Y.; Shan, J.; Zhou, H.; Li, M. Electrochemical sensor for determination of bisphenol A based on MOF-reduced graphene oxide composites coupled with cetyltrimethylammonium bromide signal amplification. *Ionics* **2020**, *26*, 3135–3146. [[CrossRef](#)]
200. Huang, H.; Chen, Y.; Chen, Z.; Chen, J.; Hu, Y.; Zhu, J.-J. Electrochemical sensor based on Ce-MOF/carbon nanotube composite for the simultaneous discrimination of hydroquinone and catechol. *J. Hazard. Mater.* **2021**, *416*, 125895. [[CrossRef](#)] [[PubMed](#)]
201. Meng, F.-L.; Guo, Z.; Huang, X.-J. Graphene-based hybrids for chemiresistive gas sensors. *TrAC Trends Anal. Chem.* **2015**, *68*, 37–47. [[CrossRef](#)]
202. Fratoddi, I.; Venditti, I.; Cametti, C.; Russo, M.V. Chemiresistive polyaniline-based gas sensors: A mini review. *Sens. Actuators B Chem.* **2015**, *220*, 534–548. [[CrossRef](#)]
203. Joshi, N.; Hayasaka, T.; Liu, Y.; Liu, H.; Oliveira, O.N.; Lin, L. A review on chemiresistive room temperature gas sensors based on metal oxide nanostructures, graphene and 2D transition metal dichalcogenides. *Microchim. Acta* **2018**, *185*, 213. [[CrossRef](#)]
204. Campbell, M.G.; Dincă, M. Metal–Organic Frameworks as Active Materials in Electronic Sensor Devices. *Sensors* **2017**, *17*, 1108. [[CrossRef](#)]
205. Koo, W.-T.; Jang, J.-S.; Kim, I.-D. Metal–Organic Frameworks for Chemiresistive Sensors. *Chem* **2019**, *5*, 1938–1963. [[CrossRef](#)]
206. Chen, X.; Li, G. Proton conductive Zr-based MOFs. *Inorg. Chem. Front.* **2020**, *7*, 3765–3784. [[CrossRef](#)]
207. Zhang, Y.; Chen, Y.; Zhang, Y.; Cong, H.; Fu, B.; Wen, S.; Ruan, S. A novel humidity sensor based on NH<sub>2</sub>-MIL-125(Ti) metal organic framework with high responsiveness. *J. Nanopart. Res.* **2013**, *15*, 2014. [[CrossRef](#)]
208. Kung, C.-W.; Platero-Prats, A.E.; Drout, R.J.; Kang, J.; Wang, T.C.; Audu, C.O.; Hersam, M.C.; Chapman, K.W.; Farha, O.K.; Hupp, J.T. Inorganic “Conductive Glass” Approach to Rendering Mesoporous Metal–Organic Frameworks Electronically Conductive and Chemically Responsive. *ACS Appl. Mater. Interfaces* **2018**, *10*, 30532–30540. [[CrossRef](#)]
209. Lee, J.-H.; Nguyen, T.T.T.; Nguyen, L.H.T.; Phan, T.B.; Kim, S.S.; Doan, T.L.H. Functionalization of zirconium-based metal–organic frameworks for gas sensing applications. *J. Hazard. Mater.* **2021**, *403*, 124104. [[CrossRef](#)] [[PubMed](#)]
210. Dmello, M.E.; Sundaram, N.G.; Singh, A.; Singh, A.K.; Kalidindi, S.B. An amine functionalized zirconium metal–organic framework as an effective chemiresistive sensor for acidic gases. *Chem. Commun.* **2019**, *55*, 349–352. [[CrossRef](#)] [[PubMed](#)]
211. Tung, T.T.; Tran, M.T.; Feller, J.-F.; Castro, M.; Van Ngo, T.; Hassan, K.; Nine, M.J.; Losic, D. Graphene and metal organic frameworks (MOFs) hybridization for tunable chemoresistive sensors for detection of volatile organic compounds (VOCs) biomarkers. *Carbon* **2020**, *159*, 333–344. [[CrossRef](#)]
212. Moghadam, B.H.; Hasanzadeh, M.; Simchi, A. Self-Powered Wearable Piezoelectric Sensors Based on Polymer Nanofiber–Metal–Organic Framework Nanoparticle Composites for Arterial Pulse Monitoring. *ACS Appl. Nano Mater.* **2020**, *3*, 8742–8752. [[CrossRef](#)]
213. Tran, H.; Feig, V.R.; Liu, K.; Zheng, Y.; Bao, Z. Polymer Chemistries Underpinning Materials for Skin-Inspired Electronics. *Macromolecules* **2019**, *52*, 3965–3974. [[CrossRef](#)]

214. Zhang, Y.; Shi, G.; Qin, J.; Lowe, S.E.; Zhang, S.; Zhao, H.; Zhong, Y.L. Recent Progress of Direct Ink Writing of Electronic Components for Advanced Wearable Devices. *ACS Appl. Electron. Mater.* **2019**, *1*, 1718–1734. [[CrossRef](#)]
215. Lawson, S.; Snarzyk, M.; Hanify, D.; Rownaghi, A.A.; Rezaei, F. Development of 3D-Printed Polymer-MOF Monoliths for CO<sub>2</sub> Adsorption. *Ind. Eng. Chem. Res.* **2020**, *59*, 7151–7160. [[CrossRef](#)]
216. Evans, K.A.; Kennedy, Z.C.; Arey, B.W.; Christ, J.F.; Schaefer, H.T.; Nune, S.K.; Erikson, R.L. Chemically Active, Porous 3D-Printed Thermoplastic Composites. *ACS Appl. Mater. Interfaces* **2018**, *10*, 15112–15121. [[CrossRef](#)]
217. Dhainaut, J.; Bonneau, M.; Ueoka, R.; Kanamori, K.; Furukawa, S. Formulation of Metal–Organic Framework Inks for the 3D Printing of Robust Microporous Solids toward High-Pressure Gas Storage and Separation. *ACS Appl. Mater. Interfaces* **2020**, *12*, 10983–10992. [[CrossRef](#)] [[PubMed](#)]